NON-STATIONARY AND CLIMATE CHANGE-INFORMED INTENSITY-DURATION-FREQUENCY (IDF) CURVE FOR THE DALLAS-FORT WORTH METROPLEX, TEXAS, UNITED STATES

by

BINITA GHIMIRE

Bachelor of Agricultural Science, 2019
Tribhuvan University
Lamjung, Nepal

Submitted to the Graduate Faculty of the
College of Science and Engineering
Texas Christian University
in partial fulfillment of the requirements
for the degree of

Master of Science

May 2023

NON-STATIONARY AND CLIMATE CHANGE-INFORMED INTENSITY-DURATION-FREQUENCY (IDF) CURVE FOR THE DALLAS-FORT WORTH METROPLEX, TEXAS, UNITED STATES

by
Binita Ghimire

Thesis approved:

Dr. Gehendra Kharel

Major Professor

Dr. Esayas Gebremichael

Dr. Linyin Cheng
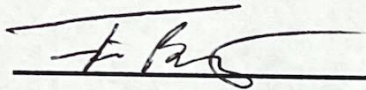
For The College of Science and Engineering

Acknowledgments

I am grateful to the following individuals and institutions who have supported me throughout my academic journey.

First and foremost, I would like to thank my thesis advisor Dr. Gehendra Kharel for his guidance, patience, and unwavering support throughout the research process. His insightful feedback and suggestions have been invaluable in shaping the direction and quality of my work.

I would also like to thank my thesis committee members, Dr. Esayas Gebremichael, and Dr. Cheng Linyin, for their time, expertise, and constructive criticism. Their thoughtful comments and questions have challenged me to think deeply about my research and helped me improve my writing.

I am grateful to the Department of Environmental and Sustainability Sciences at Texas Christian University for providing me with the resources, facilities, and funding that have enabled me to pursue my academic interests and achieve my goals.

My heartfelt thanks go to my parents, Bishow Nath Ghimire (late) and Sushila Ghimire; my grandparents Bishuhari Sapkota and Radhika Sapkota; my in-laws Toyanath Adhikari and Madhu Maya Adhikari and my family Gyan Hari Sapkota, Bijaya Sapkota, Madhu Sapkota, Namuna Pandit, and Bishal Ghimire for their unwavering love, encouragement, and support. Their belief in me has been a constant source of strength and motivation.

Finally, I want to thank my husband, Rosan Adhikari, for his unwavering love, encouragement, and support. His patience, understanding, and sacrifice have been instrumental in allowing me to pursue my academic goals. His belief in me has been a constant source of motivation and inspiration even when I doubted myself. I want to thank him for always being there for me, listening to my thoughts, and helping me see things from a different perspective. I am forever grateful for his presence in my life, and for how he has contributed to my personal and professional growth.

Once again, I want to thank everybody for their direct and indirect invaluable contributions to my academic and personal growth.

Binita Ghimire

Table of Contents

Vita

Abstract

List of Figures

List of Tables

Chapter 1: Introduction

1.1 Background

The global population has nearly tripled, from two billion in 1900 to 7.9 billion in 2020 (United Nations Department of Economic and Social Affairs, 2021). The population growth over the last century has resulted in a rapid increase in the emission of greenhouse gases (GHGs) such as carbon dioxide (CO_2), methane (CH_4), and nitrous oxides (NO_2) through rapid consumption of fossil fuels, especially in the industrialized world (Solomon et al., 2007; Weber & Sciubba, 2019). Because of that, CO_2 in the atmosphere in 2020 was 38 BMT compared to just six billion metric tons (BMT) in 1900 (Ritchie et al., 2020). As a result, the earth's atmosphere now has a cumulative CO_2 concentration of 1,655 BMT, rising from 45 BMT in 1900 (Ian, 2023). According to the Intergovernmental Panel on Climate Change (IPPC), each 1,000 BMT cumulative emission can raise the average global surface temperature by 0.27 °C to 0.63°C (IPCC, 2021). The CO_2 increase over the last century likely rationalizes the average worldwide surface temperature increase of 1.1°C since 1900 (IPCC, 2021). As a consequence of rising temperatures, the world faces climate changes leading to melting ice and glaciers, rising sea levels, and changes in precipitation patterns (Trenberth, 2011).

The global precipitation study showed that since 1901, the world's precipitation intensity has increased by an average of 0.1 inches mm per decade (NOAA, 2021). The annual maximum daily precipitation was also found to increase in almost two-thirds of the global land area since 1970 (Sarkar & Maity, 2021). Hence, the wetting trend due to the extreme precipitation is evident in central Africa, some parts of southwest Asia (e.g., Thailand, Taiwan), Central America, northern Australia, and eastern Europe between 1979 to 2010 (Damberg & Aghakouchak, 2014). The increases in precipitation are primarily seen in humid

regions of the globe, potentially increasing flood intensity in more than 75% of those regions (Tabari, 2020). A comparison study done over Europe and North America (U.S.) from 1951 to 1981 showed an increase in precipitation due to temperature rise, adding an average of 45% more extreme rainfall days between 1982 to 2013 (Fischer & Knutti, 2016). Extreme rainfall events, even shorter period (hours or days), are responsible for floods, damaging dams, roads, and storm water drainage systems (Berg et al., 2013). For example, the extreme precipitation (~203 mm in < 4 hours) incident in western Germany in July 2021 caused floods with 200 fatalities and the loss of millions of dollars' worth of properties (Dewan, 2021). Further the World Weather Attribution (WWA) noted that the intensity of extreme daily rainfall has increased by 3% to 19% compared to the preindustrial climate, which was 1.2 °C cooler than 2021, making western Germany events a 500-year occurrence events (Kreienkamp et al., 2021). Similarly, Vietnam flood incidents of 2020 due to monsoon rainfall in Khanh Hoa province were triggered by precipitation up to 360 mm in 48 hours. The tropical storm, Linfa, with 1,520 mm rainfall, further exacerbated this event by flooding more than 100,000 houses, damaging highways, caused 200 deaths, with a cumulative loss exceeding one billion United States dollars (USD) (Luu et al., 2021).

The impact of floods seems to be more severe in urban areas as they lack natural defense to flooding due to intensive land-use change associated with urban development (Allan et al., 2020; Walsh et al., 2014). Hence, the frequency and severity of flood events in the U.S. (rapidly urbanizing nation) has increased significantly due to the increase in precipitation by 5.08 mm per decade since 1900 (NOAA, 2021), which is almost twice the average global increase of 2.54 mm per decade. Similarly, the U.S. encountered several climate-related natural disasters exceeding one billion USD in losses yearly. In 2021 alone, the U.S. experienced 20

climate-related billion-dollar disaster events, out of which two were related to floods (in Louisiana and California) due to extreme precipitation (~ 381 mm in 12 hours) (NCEI, 2022). The Louisiana flood inundated around 500 buildings blocking many roads (Davis, 2021, May 19), while the California flood caused dozens of landslides and debris damaging homes, vehicles, businesses, and infrastructure, along with the washing out of the sections of a major highway, i.e., highway 1 (Smith et al., 2021).

Similarly, other devastating flood events include the 2018 flooding in North Carolina, South Carolina, and Virginia, with an average rainfall of 444.5 mm for several days, causing a \$16-\$40 billion loss of property and 53 deaths (Paul et al., 2019). These examples show the vulnerability of infrastructure, property, and lives to extreme precipitation events that have become more frequent and severe in recent decades. Engineers and planners rely on a hydrological method called the intensity-duration-frequency (IDF) curve that help design infrastructure from potential design-floods, such as 1000-year flood event.

The IDF curve is the mathematical relationship between precipitation intensity (inches per hour), or depth (inches), event duration (anywhere from a few minutes to a few days, typically 1-24 hours), and frequency, representing the average time between occurrence (e.g., once in two years, or a 50-percent chance each year). It measures how often a storm of a particular intensity occurs over a given period, which is crucial for designing drainage systems. IDF relationships were established in the 1930s (Bernard, 1932) to quantify rainfall and help plan and design various water resource projects. In 1961, Hershfield created the first geographical maps of rainfall contour to prepare rain depths for several return periods and durations (Hershfield, 1961). Nowadays, the U.S. Department of Transportation (US DOT)

uses IDF curves to assist in designing highways, culverts, bridges, and other transportation structures and estimate the volume of detention basins and their outlet structures.

Similarly, the Federal Emergency Management Agency (FEMA) uses IDF curves to produce flood maps for the U.S. (Cotter, 2018; NOAA, 2018). FEMA flood maps provide awareness about the chances of flooding in an area by dividing the space into flood risk zones, indicating the frequency and severity of flooding. Due to its broader application in infrastructure design, planning, and flood mapping, the NOAA has developed IDF curves since the 1970s (Miller et al., 1973) and published them as NOAA Atlas 14: Precipitation Frequency Atlas of the U.S. (hereafter Atlas 14). The primary purpose of Atlas 14 is to calculate annual exceedance probabilities (AEP) and average recurrence intervals (ARI) for precipitation durations ranging from 5 minutes to 60 days, with ARIs ranging from 1 to 1,000 years. AEP is the chance or probability of a flooding event occurring annually, while ARI explains how often the particular precipitation events have occurred in the past. Both ARI and AEP indicate the likelihood of a specific amount of precipitation with a certain potential of a flood occurring in the future.

Atlas 14 is published and updated periodically (Bonnin et al., 2006). The updates include more recent and extended precipitation data sets, currently accepted statistical approaches, and improved spatial interpolation and mapping techniques. For example, the most recent Atlas 14 update was released in 2018 for Texas, including rainfall records from the 1870s to 2017, and published as volume 11, version 2 (Perica et al., 2018). The updated Atlas 14 for Texas showed increased precipitation amounts compared to the older version developed using precipitation data until 2001. For example, in Austin, Texas, a 100-year 24-hour rainfall increased by 76 mm, and events previously categorized as 100-year occurrences have now

become 25-year events. However, besides some changes in Atlas 14, the update is still based on historical data with assumed stationarity in the precipitation data, which may need to be revised to reflect a potential future projected increase in precipitation and non-stationarity of rainfall data. It is because studies done in different parts of the world support changes in IDF curve characteristics under future precipitation scenarios and non-stationary assumptions. For instance, a study done in Canada compared the future-based IDF curve under the non-stationary assumption with the historical data-based IDF curve under the stationary assumption. The authors found that the historical data-based IDF curve underestimated the flood probability leading to an increase of projected hazards in the future by 257% to 443%, warning of severe impact on society and infrastructure safety (Silva et al., 2021).

Similarly, the history of repeated flood incidents in the U.S. and its area under flood zone estimated by FEMA also indicate a change in precipitation intensity and incompetency of available IDF curves. For example, more than 200,000 houses were damaged during Hurricane Harvey, of which only one-fourth were listed in the flood-prone zone (Amadeo, 2018). During Hurricane Katrina, severe flood damage to Alabama, Louisiana, and Mississippi structures was outside the flood risk zone (Team, 2006). A study done to estimate the U.S. population exposed to food risk of 100-year storm events estimated 40.8 million U.S. residents were exposed, which is 69% higher than the FEMA estimation of only 13 million (Wing et al. 2018), manifesting the underestimation of Atlas 14.

Nevertheless, NOAA has yet to change its standardized approach to deriving the Atlas 14, i.e., based on historical precipitation data and stationary assumptions till now. Under stationary assumptions, it assumes that the average and variance of precipitation data remain consistent over time. In other words, stationary assumption means an event with the return

level of T-year will have a 1/T chance of occurrence in every given year, and there will be no change in the frequency of event occurrence over time (Klein Tank & Können, 2003). Generally, Atlas 14 is developed by fitting precipitation data on generalized extreme value (GEV) based on annual maximum precipitation series (AMS), the largest rainfall recorded annually at a particular location or station (Coles et al., 2001) or generalized Pareto distribution (GPD) based on peaks-over-threshold (POT) extremes (IPCC, 2002). GEV distributions are commonly used to represent probability density functions (PDFs) of AMS events. Once GEV is fitted, the distribution can be inverted to calculate the magnitude of an event with any specified recurrence interval. The GEV distribution is characterized by three parameters: location (μ), scale (σ), and shape (ξ). However, GEV and GPD calculation methodologies will differ when considering non-stationary assumptions. Most commonly, the non-stationary model is applied to the GEV location parameter (μ). With stationarity, it is assumed that precipitation data will not show any increasing or decreasing trend. In other words, the data's location parameter (μ) does not vary with time. However, many studies have widely observed increasing trends in extreme precipitation, even in places where total precipitation is not changing (Easterling et al., 2017) (Kunkel, 2003), 2003; Groisman (Groisman et al., 2005) (Alexander et al., 2006).

Moreover, with climate change, a naturally occurring process, which has been amplified since the industrial revolution due to increased anthropogenic activities, precipitation is conspicuously becoming non-stationary. Therefore, developing an IDF curve with a stationarity assumption may make the utility of such IDF curves questionable and less reliable for infrastructure design. Cheng et al. (2014) also supported that using stationary assumptions could lead to the underestimation of extreme precipitation events by up to 60%,

6

increasing the risk of infrastructure failure due to floods. Similarly, Soulis et al. (2016) compared extreme precipitation trends in Ontario, Canada, from 1960 to 2010 and observed that under non-stationary conditions, the intensity of extreme precipitation for 30-minute and 24-hour storms increased by 1.25% and 1.82% per decade, respectively.

Several studies have considered non-stationary assumptions to calculate changes in different duration-frequency values. For example, Wi et al. (2016) applied non-stationary GEV and GPD models to analyze extreme precipitation frequency in South Korea. They found that the stationary model underestimated design storms for all return periods compared to the non-stationary model. While comparing GEV and GPD non-stationary models, the design storm estimated by GPD was generally smaller than the estimate derived from GEV. Cooley et al. (2007) used a spatiotemporal Bayesian hierarchical modeling approach to develop the IDF curve in Colorado. They produced IDF curves of various return periods, including features that the 1973 NOAA atlas left out. Cheng et al. (2014) developed a Bayesian-based framework to analyze non-stationary precipitation extremes. They found an increase in exceedance probability by 60% under the non-stationary climate. Towler et al. (2010) used a non-stationary GEV method to model future precipitation extremes in streamflow and turbidity of Bull Run Watershed in Oregon. They found more than a percentage increase in the portability of exceeding a turbidity threshold from 4.2% to 5.4%.

In addition to the stationary assumption, the sole dependence of Atlas 14 on historical precipitation makes it potentially less adaptive to climate change. It is because global climate models (GCMs) project further increases in extreme precipitation events in terms of intensity and frequency over the next several decades in many parts of the U.S. (Arias et al., 2021). GCMs provide precipitation projections under different emission scenarios. Although GCMs

exhibit uncertainty, they offer plausible scenarios of future climatic conditions and can be used to derive future IDF curves. Extreme precipitation projections of GCMs tend to follow the scaling of Clausius-Clapeyron, i.e., a 1°C rise in temperature could increase extreme precipitation by increasing the moisture holding capacity of air by approximately 7% (Pendergrass et al., 2015). Several studies done in the U.S. and other regions showed increased precipitation intensity in IDF curves based on GCM projected future precipitation data. For example, Ragno et al. (2018) used precipitation projections of 19 GCMs from the Coupled Model Inter-comparison Project Phase 5 (CMIP5) to derive IDF curves for 14 major cities in the U.S. They observed that highly populated areas in the U.S. are likely to experience extreme precipitation events up to 20% more intense and twice as frequent relative to NOAA developed historical precipitation-based Atlas 14. Similarly, in the Chesapeake Bay Watershed and Virginia, the IDF curves were developed using climate data from 78 GCMs under two representative concentration pathway (RCP) scenarios- RCP4.5 & RCP8.5 for two future periods, 2020-2069 and 2050-2099. They found an 8 to 20% increase in rainfall intensities compared to the historical climate (Miro et al., 2021). Houck & Board (2019) used 20 CMIP5 GCM precipitation projections to develop climate-adjusted IDF curves for Colorado. The authors found that 24-hour, 100-year precipitation intensity is likely to increase by 10 to 20% across the state by 2050. In addition, different studies conducted in various places of the globe using projected precipitation data found an increase in rainfall intensities for all return periods (Cannon & Innocenti, 2019; Shrestha et al., 2017; Tien Thanh & Dutto Aldo Remo, 2018). However, Shukor et al. (2020) found a decrease in future intensities for longer return periods of 50-year and 100-year but an increase in intensities for the shorter and medium return periods of 2, 5, 10, and 25 years in the state of Kelantan, Malaysia. Hence, excluding future projected

GCM precipitation data in Atlas 14 might potentially expose our drainage system and infrastructure to elevated risk (Vahedifard et al., 2017). Therefore, sole dependence on historical data and stationarity assumption in the current IDF curve development are critical limitations of Atlas 14, potentially leading to unreliable estimates of extreme events.

1.2 Objectives

Thus, the primary purpose of this study is to develop IDF curves incorporating non-stationary assumptions and also including future projected GCM precipitation, then compare those IDF curves with Atlas 14 to quantify the potential changes and provide insight into the need for augmentation of Atlas 14. A study by Emanuel (2017) for Texas found that 100-year rainfall is estimated to increase by 18% by the end of the century compared to the 1981-2000 period under the IPCC high-emission scenario. For this project, Dallas-Fort Worth (DFW) metroplex, the largest metropolitan region in Texas, was selected as the study area. The study findings, non-stationary and future projected climate-based IDF curves, could provide an informed tool to stormwater engineers and planners in infrastructure design and risk assessment consistent with future precipitation conditions for the DFW metroplex. To achieve the study objective, following specific objectives were carried out:

- To acquire AMS from NOAA for all stations in the DFW metroplex.

- To conduct a statistical trend test of AMS to determine stations showing the non-stationary trend.

- To acquire AMS of GCM-based projected precipitation data for the selected stations.

- To develop IDF curves based on non-stationary assumption.

- To develop IDF curves using GCM projected future precipitation data.

- To compare non-stationary and climate change-based IDF curves with the Atlas14.

Chapter 2: Methodology

2.1 Study Area

The DFW metroplex (Figure 1) lies in north central Texas, with 16 counties covering an area of 12,741 mi^2 (~33,000 km^2), including two major cities (Dallas and Fort Worth) and more than 100 smaller cities with a population of ~7.6 million (US Census Bureau's 2020 census). Furthermore, by 2030 the population of DFW is projected to reach 9.1 million. Comparing the 1.52% population growth rate (PGR) in the DFW area in 2021 with the 1.1% for Texas and 0.58% for the U.S., the DFW metroplex is one of the fastest-growing urban areas in the U.S. (Macro Trends, 2023). Subsequently, such an increase in urban population leads to growth in urban development, causing more impervious surfaces, which increase storm overland flow, making urban areas vulnerable to flooding (Feng et al., 2021).

Despite being a drought-prone area with an annual average of ~36 inches of rainfall, the DFW metroplex has been subjected to flooding on several occasions due to extreme precipitation events. The long-term precipitation trend for the area indicates an increase in rainfall of 15 % from 1900 to 2010 (Winguth et al., 2015). In particular, extreme precipitation increased by ~7% between 1960 and 2020 (Nielsen-Gammon et al., 2020). For example, on May 24, 1986, Fort Worth, the 2nd largest city in the DFW metroplex, received 3.5 inches of rainfall in an hour, causing flash flooding that cost $2 million in damages and caused two fatalities (Lanning-Rush et al., 1998). Since then, the DFW metroplex has experienced at least four other extreme precipitation events. On May 24, 2014, three inches of precipitation fell within 90 minutes, leading to flooding of roads and infrastructure. On May 24, 2015, three inches of rainfall was recorded within 24 hours, with a total of 16.5 inches that month, making it the wettest May on record (Chris, 2015). This unusually high storm event resulted in

flooding and accrued an estimated $1 billion in insured losses, with vehicle damages accounting for ~25% of the total cost. Also, Dallas, the largest city in the DFW metroplex, reported an additional $50 million in losses because of localized flooding of parks and roads and the cost of debris removal (North Central Texas Floods May-June 2015). On January 16, 2020, four inches of precipitation fell within 24 hours in the region, causing flash floods and most recently, according to the record of Dallas Water Utilities, on August 22, 2022, some parts of DFW recorded > 13 inches of rainfall in 24 hours (Dey & Douglas, 2022). According to the current precipitation frequency estimates from NOAA, the latter storm event had a 0.1% chance of happening in a year as they were on a 1000-year flood event (Dey & Douglas, 2022). Such storm events in the last few decades exemplify that the DFW area is not only subject to extreme precipitation events but there is also an increasing trend toward these events, causing potentially elevated flood risks. Thus, Atlas 14, which is based on historical precipitation data and stationary assumption, may not provide adequate information to develop infrastructures resilient to non-stationary precipitation trends and projected increases in precipitation due to climate change. Therefore, this study aims to develop a climate change informed IDF tool for the DFW region.
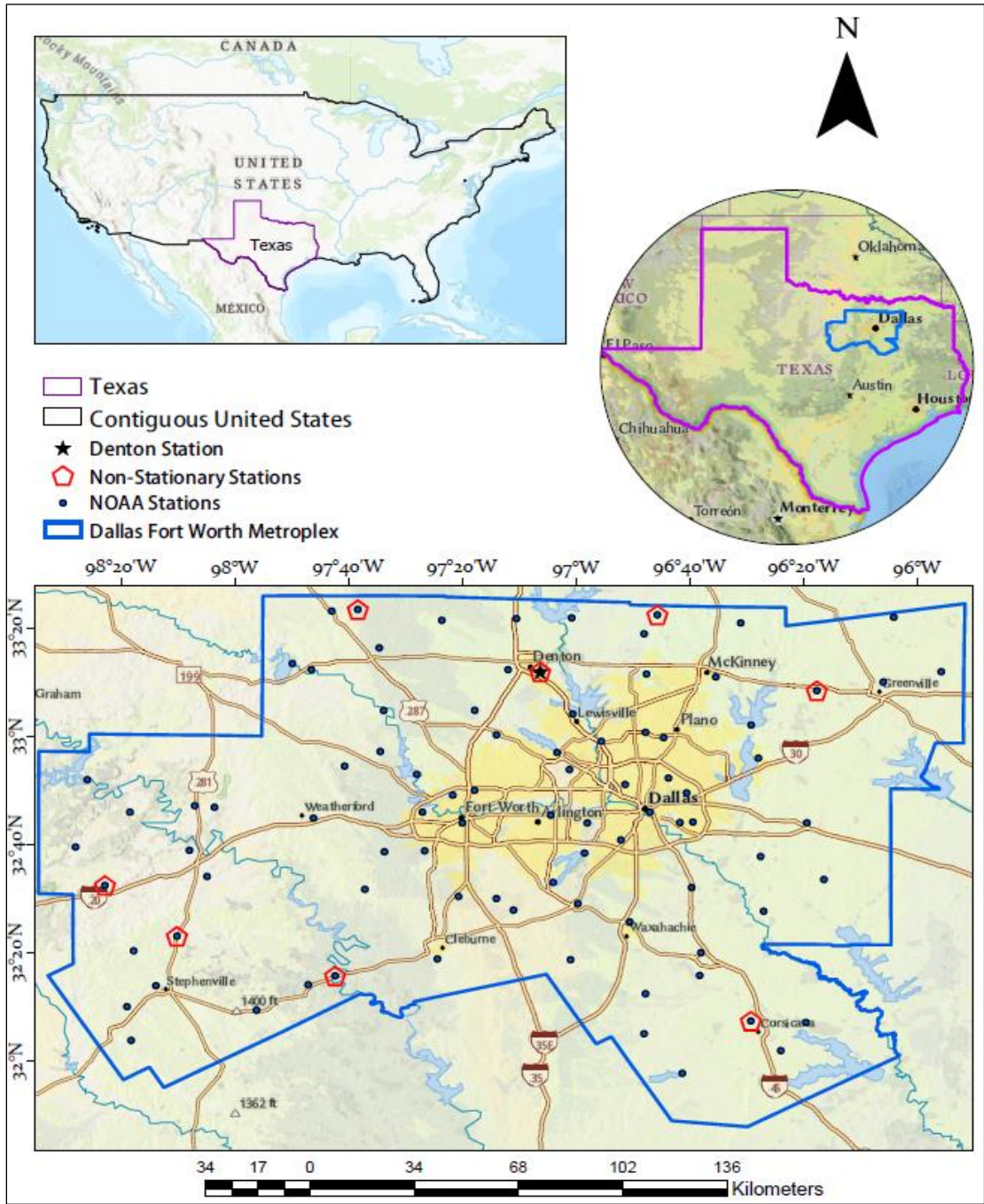
Figure 1: The study area is the Dallas-Fort Worth metroplex (DFW) located in north central Texas, United States with precipitation stations represented by blue dots, non-stationary trend exhibiting stations (red pentagons) and Denton station (black star) used for future climate-based tool development

2.2 Data and Data Source

This study made use of daily AMS of (i) the historical precipitation data used by NOAA to develop their IDF curves or Atlas 14 (Perica et al., 2018) and (ii) daily GCM-projected precipitation data (Figure 2). AMS data from 88 stations located in the study area boundaries were extracted from NOAA Precipitation Frequency Data Server (PFDS) via their web portal (https://hdsc.nws.noaa.gov). However, GCMs' daily data for 2040-2099 were downloaded for the Denton station (Figure 1), which shows a non-stationary trend in historic-precipitation data and also is located in one of the fasted growing regions in DFW.

GCMs data from the Multivariate Adaptive Constructed Analogs (MACA) climatology lab (Abatzoglou & Brown, 2012) were selected for this study because the data were already downscaled and bias-corrected with a 4 km resolution available for DFW metroplex. Also, MACA includes RCP4.5 and RCP8.5 projections, the two most used RCPs in climate adaptation literature and practices. RCP4.5 is often interpreted as an optimistic future with low emissions (Thomson et al., 2011) while RCP8.5 is closer to a worst-case future with higher emissions (Riahi et al., 2011).

While assessing future conditions, there is always huge uncertainty about the variation of the data, so more GCMs may be needed to capture changes in precipitation and reduce GCM-specific uncertainties. Therefore, all available 20 GMCs in MACA were used in this study. These GCMs include (1) Bcc-csm1-1, (2)Bcc-csm1-1-m, (3) BNU-ESM, (4) CanESM2, (5) CCSM4, (6) CNRM_CM5, (7) CSIRO-Mk3-6-0, (8) GFDL-ESM2M, (9) GFDL-ESM2G, (10) HadGEM2-CC365, (11) HadGEM2-ES365, (12) inmcm4, (13) IPSL-CM5A-LR, (14) IPSL-CM5A-MR, (15) IPSL-CM5B-LR, (16) MIROC5, (17) MIROC-ESM, (18) MIROC-

ESM-CHEM, (19) MRI-CGCM3, (20) NorESM1-M. Detailed information about the MACA

product and methodology was discussed in Abatzoglou & Brown (2012).
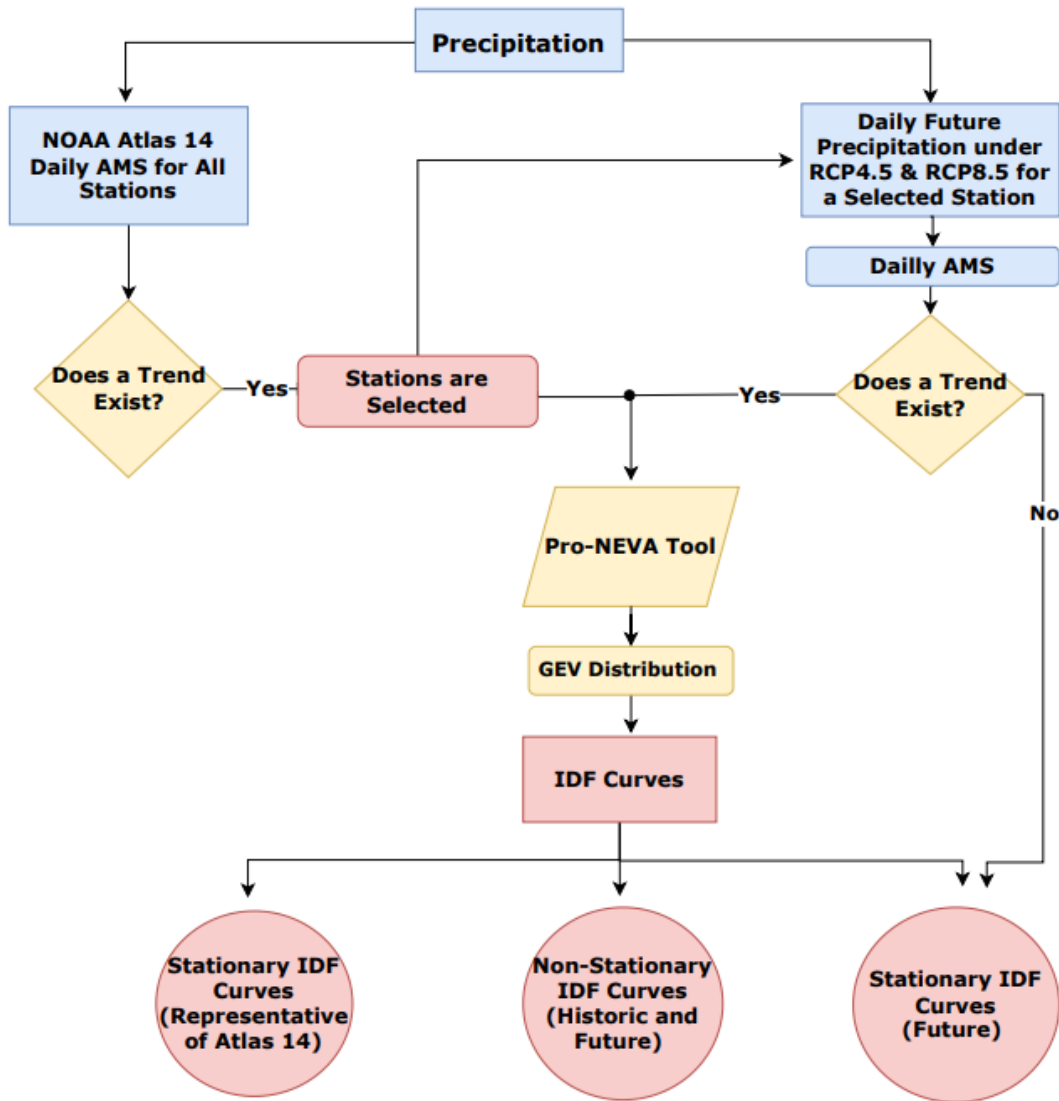
Figure 2: A schematic diagram showing the general methodology to develop intensity-duration-frequency (IDF) curves based on non-stationary assumption and future climate for the Dallas-Fort Worth metroplex

2.3 Methods

The study methodology is shown in Figure 2 and include the following key steps:

2.3.1 Extraction of AMS

IDF curves are developed using the extreme or largest rainfall values. Hence, following the methods of Atlas 14 (Perica et al., 2018), for developing historical IDF curves, daily duration AMS data of 88 stations in the study area were used. For the future climate, only one station (Denton) was used as a representative station, and therefore AMS was extracted for a 2040- 2099 period for 20 GCMs under RCP4.5 and RCP8.5 using equation 1.

$$P_{d,max}^{j} = max \left\{ \frac{\sum_{t=1}^{d} p_t^{j}}{d}, \dots, \frac{\sum_{t=1}^{i+d-1} p_t^{j}}{d}, \dots, \frac{\sum_{t=n_{j-d+1}}^{n_j} p_t^{j}}{d} \right\} \qquad 1$$

2.3.2 Trend Test

To determine whether extracted AMS follows the stationary or non-stationary trend, various statistical tests such as Augmented Dickey-Fuller (ADF) (Cheung & Lai, 1995), Kwiatowski-Phillips-Schmidt (KPSS) (Kwiatkowski et al., 1992), Phillips-Perron (PP) (Phillips & Perron, 1988), Mann-Kendall (MK) (Kendall, 1948; Mann, 1945), Pettitt (PT) (Pettitt, 1979), Ljung-Box (LB) (Ljung & Box, 1978), Zivot-Andrews (ZA) (Zivot & Andrews, 2002), Elliot-Rothenberg-stock (ERS) (Elliott et al., 1992), Variance Ratio (VR) (Chow & Denning, 1993), and Wavelet-based (Von Sachs & Neumann, 2000) can be used. However, the use of trend tests is based on the specific characteristics of the time series being analyzed and the research question being addressed. Also, researchers suggested to use multiple tests to confirm the stationarity or non-stationarity of a time series (Prosdocimi et al., 2014; Um et al., 2018). So, for this study, five null-hypothesis significance trend tests, popularly used in hydrology and extreme analysis, were chosen. Trend tests were conducted for the AMS data

of all 88 stations NOAA used to develop Atlas 14 for the DFW metroplex. Then, only those stations that exhibited a trend in at least two out of five tests were selected for the next step of developing IDF curves under non-stationary condition (Figure 2). Similarly, a trend test was performed for the AMS of each GCM under both RCPs for the Denton station. GCMs that showed non-stationary trends were used to develop future climate-based IDF curves assuming non-stationarity. For other GCMs showing no trend, future climate-based IDF curves were generated assuming a stationary condition (Figure 2).

2.3.2.1 Mann-Kendall Trend Test

Mann-Kendall (MK) trend test is a non-parametric statistical test for time series data to check the presence of a monotonous trend of increasing or decreasing over time (Kendall, 1948; Mann, 1945). Hence, data that violate the normal distribution condition can be used to perform the MK trend test. MK test is a ranked-based test, so it is considered robust against outliers. It can be carried out at the user's choice significance level. In the MK test, the null hypothesis of "no trend in the time series" is rejected if the test statistic p-value is smaller than the critical value $Z\alpha$. In this study, the test was carried out at a 5% significance level, so if the p-value was less than 0.05, it would indicate that the AMS data showed a non-stationary trend.

2.3.2.2 Pettitt Test

Pettitt Test is also ranked based on a non-parametric statistical test that measures the change point in the time series data (Pettitt, 1979). In the Pettitt Test, the null hypothesis of "no change point or two distributions of data are equal" is rejected if the p-value is smaller than the critical value $Z\alpha$. This study used a 5% significance level. Therefore, the p-value less than 0.05 indicates that the time series data has a change point and follows a non-stationary trend.

2.3.2.3 Kwiatkowski–Phillips–Schmidt–Shin Test

Kwiatkowski–Phillips–Schmidt–Shin (KPSS) test is a null hypothesis test to find if a time series shows stationarity around a deterministic trend (Kwiatkowski et al., 1992). Unlike other unit root tests, it proposes that the time series data has a unit root, i.e., a non-stationary trend in an alternative hypothesis. In contrast, its null hypothesis is that the time series data is stationary. At the 5% significance level, if the p-value is less than 0.05, then the null hypothesis is rejected, implying data the data has a non-stationary trend. The KPSS test has a high rate of Type 1 error as it tends to reject null hypothesis quite frequently; therefore, a combination of Augmented Dickey Fuller tests is recommended to reduce such errors.

2.3.2.4 The Augmented Dickey-Fuller Test

The Augmented Dickey Fuller (ADF) is a unit root test for stationarity (Cheung & Lai, 1995). Unit root in the time series data indicates a non-stationary trend. So, the null hypothesis for the test is that there is a unit root, i.e., a non-stationary trend, and the alternative hypothesis is that the time series data is stationary. So, at the 5% significance level, if the p-value is greater than 0.05, the null hypothesis is retained, indicating that the time series data is non-stationary.

2.3.2.4 The Phillips–Perron Test

The Phillips–Perron (PP) test is also a unit root test. It is used in non-parametric time series analysis to test the null hypothesis that a time series is an integration of order one (Phillips & Perron, 1988). At the 5% significance level, if the p-value is greater than 0.05, the null hypothesis cannot be rejected, indicating that the time series has a non-stationary trend.

2.3.3 IDF Curves Development

In this research, only 24-hour duration IDF curves were developed using ProNEVA software (Ragno et al., 2019) because 24-hour duration is one of the most commonly used

durations for assessing rainfall intensity and designing drainage systems. It is also a duration of interest for flood management in many areas. Therefore, developing future climate and non-stationary IDF curves for 24-hour duration, crucial duration, can be a good starting point in assessing the impact of changing climate on rainfall patterns in the DFW metroplex. As the 24-hour duration is a common and important duration in hydrological and hydraulic engineering, it can be argued that assessing the performance of the Atlas 14 based on historic data and stationary assumption using 24-hour duration is a reasonable approach. Additionally, since developing IDF curves for longer durations may require longer periods of data, which may not be available or reliable, using the 24-hour duration can be a practical choice for assessing the impact of changing climate on rainfall patterns in the DFW metroplex.

2.3.3.1 ProNEVA Tool

Process-informed Non-stationary Extreme Value Analysis (ProNEVA) is a statistical modeling framework developed to estimate the frequency and magnitude of extreme events, such as floods and droughts, under stationary and non-stationary conditions. ProNEVA is a modified and the most recent version of the NEVA tool developed by Cheng etal. (2014). ProNEVA has the option to choose from three different extreme value distribution analysis functions, namely (i) the GEV, (ii) the GP, and (iii) the Log-Pearson Type III (LP3). Among these three, GEV distribution is commonly used to model the distribution of extreme events (Hossain et al., 2021; Park et al., 2011; Rypkema & Tuljapurkar, 2021; Zalina et al., 2002). Moreover, NOAA also recommends using the GEV distribution, and therefore NOAA used the GEV distribution function to develop Atlas 14 (Perica et al., 2018). Because of these two reasons and to be comparable with Atlas 14, the GEV distribution was used in this study (Figure 2). The GEV distribution is a measure based on three distribution parameters as

explained by θ=(μ,σ,ξ), where, the location parameter (μ) specifies the center of the distribution, the scale parameter (σ) determines the size of deviations around the location parameter; and the shape parameter (ξ) governs the tail behavior of the GEV distribution. In this study, the location and scale parameters were assumed to be a linear function of time to account for non-stationarity while keeping the shape parameter constant because the shape parameter is known to be difficult to precisely estimate even in the stationary case (Coles et al., 2001; Ragno et al., 2019).

Pro-NEVA uses the Bayes theorem for estimating GEV parameters under the non-stationary assumption. The Bayes theorem states that the probability of an event occurring given some prior knowledge and new evidence is proportional to the product of the prior probability and the likelihood of the evidence given the event (Swinburne, 2004). Bayes approach is beneficial in situations where we have incomplete or uncertain information and need to make decisions based on probabilities (Barber, 2012). It also offers uncertainty of the parameter estimates, yielding more realistic estimations (Robert, 2007). Mathematically, it can be expressed as equation 2. For more information about the Bayes Theorem, see Bernardo & Smith (2001). Cheng et al. (2014) provides detailed explanations of the application of the Bayes Theorem in generating non-stationary IDF curves.

$$p\left(\beta \mid \overrightarrow{y}, x\right) \propto \mathrm{P}(\overrightarrow{y} \mid \beta, x)p(\beta \mid x)$$

$$p\left(\beta \mid \overrightarrow{y}, x\right) = \Pi\, \boldsymbol{P}(\boldsymbol{y_t} \mid \beta, x(t)) = \Pi p(\boldsymbol{y_t} \mid \boldsymbol{\mu(t)}, \boldsymbol{\sigma}, \boldsymbol{\xi}) \qquad 2$$

Where y(t) denotes the set of all covariate values under the non-stationary assumption, and stationarity can be treated as a particular case without the term y(t). The resulting posterior

distributions provide information on the distribution parameters (µ1, µ0, σ, ξ) (Cheng & Aghakouchak, 2015).

2.3.3.2. Non-Stationary and Stationary IDF Curves

Non-stationary assumption-based IDF curves were developed for seven stations (Figure 1) using the historical AMS data for each station as used by NOAA in developing Atlas 14 and by applying the GEV distribution to be consistent with the method used in Atlas 14 (Figure 2). As the ProNEVA tool uses Bayes theorem for estimating GEV, prior parameters (µ,σ,ξ) values were calculated for each station as listed in

Table 1 and were used to develop IDF curves for each station. This study used time as a covariate for the non-stationary assumption. Since Atlas 14 is based on the stationarity assumption, stationary-based IDF curves were also developed for each station to represent Atlas 14.

Table 1: Prior parameters as input to the ProNEVA tool for the generalized extreme value distribution-based intensity-duration-frequency (IDF) curves for seven non-stationary stations

Precipitation Station	Parameter values used in ProNEVA					
	Location (μ)		Scale (σ)		Shape (ξ)	
Corsicana	3.6	1.7	0.0	5.0	-0.35	0.35
Denton 2 SE	3.5	1.5	0.0	5.0	-0.35	0.35
Farmersville	3.9	1.0	0.0	5.0	-0.35	0.35
Gordon 1SW	3.4	1.4	0.0	5.0	-0.35	0.35
Gunter 5S	3.9	1.6	0.0	5.0	-0.35	0.35
Morgan Mill	3.5	1.6	0.0	5.0	-0.35	0.35
Rainbow	3.3	1.2	0.0	5.0	-0.35	0.35

2.3.3.3 IDF curves based on GCM Projections

IDF curves based on GCMs were developed only for the Denton station as a representative station for the study area. Also, Denton is located in the most rapidly urbanizing region of the DFW metroplex. In addition, NOAA also points out non-stationarity trend in the AMS data of the Denton station but still did not consider while developing IDF curves (Perica et al., 2018), which could be a reasonable basis for conducting a comparison study.

Future IDF curves were developed using stationary and non-stationary conditions based on the trend test result. For GCMs that showed a non-stationary trend in the trend tests, IDF curves were created using the non-stationary assumption. For the rest of the GCMs, future IDF curves were developed using the stationary assumption. Like the historical AMS, time was used as a covariate for the non-stationary assumption. For each GCM under RCP8.5, their prior parameter information was calculated and used to develop IDF curves, as shown in Table 2.

Table 2: Prior parameters input to run generalized extreme value distribution for different GCMs of Denton station under RCP8.5 scenario

GCMs	Prior parameter values used in ProNEVA					
	Location (μ)		Scale (σ)		Shape (ξ)	
Bcc-csm1-1-m	3.12	1.09	0.00	5.00	-0.35	0.35
Bcc-csm1-1	3.25	1.13	0.00	5.00	-0.35	0.35
BNU-ESM	2.65	0.73	0.00	5.00	-0.35	0.35
CanESM2	3.07	1.68	0.00	5.00	-0.35	0.35
CCSM4	2.68	0.71	0.00	5.00	-0.35	0.35
CNRM_CM5	3.10	1.41	0.00	5.00	-0.35	0.35
CSIRO-Mk3-6-0	3.21	1.61	0.00	5.00	-0.35	0.35
GFDL-ESM2G	2.91	1.05	0.00	5.00	-0.35	0.35
GFDL-ESM2M	3.01	1.69	0.00	5.00	-0.35	0.35
HadGEM2-CC365	2.73	0.86	0.00	5.00	-0.35	0.35
HadGeM2-ES365	2.97	1.28	0.00	5.00	-0.35	0.35
inmcm4	2.49	0.76	0.00	5.00	-0.35	0.35
IPSL-CM5A-LR	3.13	1.39	0.00	5.00	-0.35	0.35
IPSL-CM5A-MR	2.57	1.18	0.00	5.00	-0.35	0.35
IPSL-CM5B-LR	3.14	1.05	0.00	5.00	-0.35	0.35
MIROC-ESM-CHEM	2.87	0.92	0.00	5.00	-0.35	0.35
MIROC-ESM	3.40	1.10	0.00	5.00	-0.35	0.35
MIROC5	2.66	0.89	0.00	5.00	-0.35	0.35
MRI-CGCM3	2.74	1.26	0.00	5.00	-0.35	0.35
NorESM1-M	2.55	0.90	0.00	5.00	-0.35	0.35

For each GCM under RCP4.5, their prior parameter information was calculated and used to develop IDF curves, as shown Table 3.

Table 3: Prior parameters input to run generalized extreme value distribution for different GCMs of Denton station under RCP4.5 scenario

GCMs	Prior parameter values used in ProNEVA					
	Location (μ)		Scale (σ)		Shape (ξ)	
Bcc-csm1-1-m	2.80	0.96	0.00	5.00	-0.35	0.35
Bcc-csm1-1	3.20	1.14	0.00	5.00	-0.35	0.35
BNU-ESM	2.84	0.94	0.00	5.00	-0.35	0.35
CanESM2	2.68	1.25	0.00	5.00	-0.35	0.35
CCSM4	2.80	1.12	0.00	5.00	-0.35	0.35
CNRM_CM5	2.86	1.32	0.00	5.00	-0.35	0.35
CSIRO-Mk3-6-0	3.29	1.64	0.00	5.00	-0.35	0.35
GFDL-ESM2G	2.98	1.12	0.00	5.00	-0.35	0.35
GFDL-ESM2M	2.83	1.20	0.00	5.00	-0.35	0.35
HadGEM2-CC365	3.06	1.62	0.00	5.00	-0.35	0.35
HadGeM2-ES365	2.74	1.27	0.00	5.00	-0.35	0.35
inmcm4	2.93	1.18	0.00	5.00	-0.35	0.35
IPSL-CM5A-LR	3.12	1.44	0.00	5.00	-0.35	0.35
IPSL-CM5A-MR	2.84	1.18	0.00	5.00	-0.35	0.35
IPSL-CM5B-LR	3.18	1.28	0.00	5.00	-0.35	0.35
MIROC-ESM-CHEM	2.81	0.95	0.00	5.00	-0.35	0.35
MIROC-ESM	3.25	1.06	0.00	5.00	-0.35	0.35
MIROC5	2.82	1.13	0.00	5.00	-0.35	0.35
MRI-CGCM3	2.98	0.86	0.00	5.00	-0.35	0.35
NorESM1-M	2.49	0.92	0.00	5.00	-0.35	0.35

2.4. Analysis

Using historical AMS, IDF curves were developed under non-stationary and stationary conditions for seven stations. As explained earlier, non-stationary and stationary IDF curves were generated for one station using GCM-based AMS. Then, the resulting IDF curves were compared to see if any differences could be observed in terms of changes in the intensity of

storm events for a particular return period (e.g., a 24-hour, 100-year storm event). For each station, the percentage change in the intensity of extreme precipitation of the non-stationary-based IDF curves was calculated against Atlas 14 of the respective station. Similarly, for the Denton station, the percentage change in the intensity of extreme precipitation of the 20 different future climate-based IDF curves developed using non-stationary or stationary assumptions was calculated against Atlas 14 of the same station.

Chapter 3: Results

3.1 AMS Comparison

A box plot was created to visually compare the distribution of extreme rainfall events for seven stations with non-stationary rainfall trends over time, as shown in Figure 3. Analysis
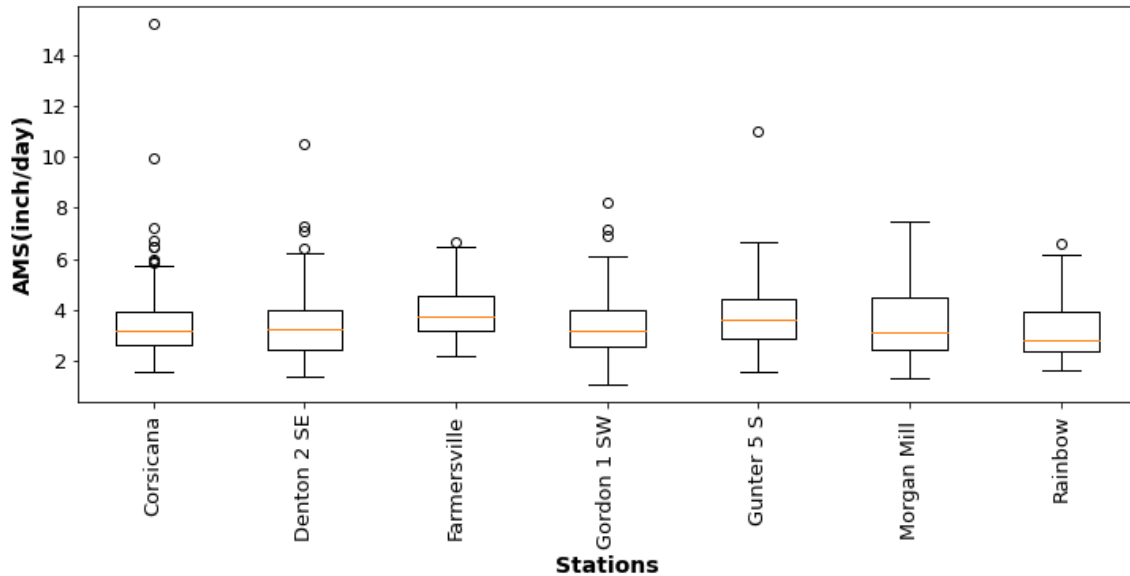
Figure 3: A side-by-side box and whisker plot of annual maximum series (AMS) of seven non-stationary precipitation stations in the Dallas-Fort Worth metroplex

of the AMS for seven stations showed that, except for Morgan Mill station, all other stations had received at least one much higher one-day extreme precipitation event, as considered an outlier in the box plot, than the typical range of the data. The highest count of outliers was observed at Corsicana, followed by Denton and Gordon (Figure 1). Similarly, Corsicana had once received much higher one-day extreme precipitation (> 14 inches/day) than other stations. However, while comparing the median, Corsicana station had a lower median AMS than Farmersville and Gunter, as shown in Table 4 . When comparing the whiskers of each station, it was found that all stations had upper whiskers longer than lower whiskers, meaning the AMS values for all seven stations were positively skewed or right-tailed. In addition, the mean value

higher than the median value and a positive value for the skewness coefficient indicates that all seven stations are right-tailed, as shown in Table 4. Among all stations, Farmersville had the smallest range of extreme AMS values without outliers, while Morgan Mill had the largest range of typical extreme AMS values without outliers. Corsicana has the longest range of extreme AMS values with outliers and the highest skewness, as shown in Table 4.

Table 4: Descriptive statistic of the annual maximum series of seven stations in the Dallas-Fort Worth metroplex

Stations	Mean	Median	Standard Deviation	Skewness Coefficient
Corsicana	3.59	3.21	1.67	3.62
Denton 2 SE	3.52	3.23	1.46	1.63
Farmersville	3.92	3.77	1.03	0.67
Gordon 1 SW	3.41	3.19	1.40	1.23
Gunter 5 S	3.87	3.65	1.57	1.89
Morgan Mill	3.54	3.15	1.59	0.90
Rainbow	3.27	2.85	1.23	0.93

The comparison between the historical and GCM AMS values of the Denton station (Figure 4 & Figure 5) showed that some GCMs have much higher one-day extreme precipitation events (outliers) compared to the historical AMS values.

Under RCP4.5, CNRM_CM5 has much higher one-day extreme precipitation events (> 12 inches/day) than historic AMS outliers (11 inches/day). However, while comparing the median value, it was observed that the historical AMS had higher median values (3.2 inch/day) than that of GCMs, as shown in Table 5. In addition, similar to the historical AMS, all GCM AMS values were positively skewed, i.e., right-tailed, as shown in Figure 4 and Table 5.

Table 5: Descriptive statistics of annual maximum series of GCMs under RCP4.5 at the Denton station

GCMs	Mean	Median	Standard Deviation	Skewness Coefficient
Stations	3.5	3.2	1.5	1.6
Bcc-csm1-1-m	2.8	2.8	1.0	1.7
Bcc-csm1-1	3.2	2.9	1.1	0.8
BNU-ESM	2.8	2.7	0.9	1.0
CanESM2	2.7	2.4	1.2	2.6
CCSM4	2.8	2.4	1.1	1.5
CNRM_CM5	2.9	2.5	1.3	2.2
CSIRO-Mk3-6-0	3.3	3.0	1.6	3.5
GFDL-ESM2G	3.0	2.8	1.1	0.6
GFDL-ESM2M	2.8	2.6	1.2	1.5
HadGEM2-CC365	3.1	2.7	1.6	3.5
HadGEM2-ES365	2.7	2.3	1.3	2.2
inmcm4	2.9	2.7	1.2	1.5
IPSL-CM5A-LR	3.1	2.9	1.4	1.5
IPSL-CM5A-MR	2.8	2.7	1.2	1.1
IPSL-CM5B-LR	3.2	3.0	1.3	3.1
MIROC-ESM-CHEM	2.8	2.8	0.9	0.9
MIROC-ESM	3.3	2.9	1.1	0.6
MIROC5	2.8	2.6	1.1	1.8
MRI-CGCM3	3.0	2.9	0.9	0.2
NorESM1-M	2.5	2.4	0.9	1.6
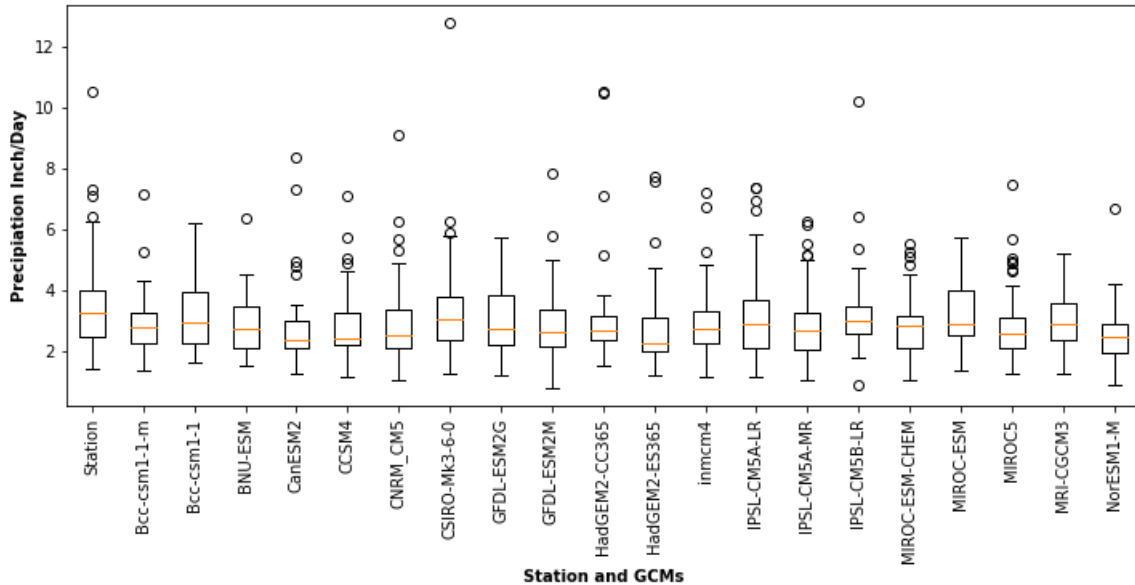
Figure 4: A side-by-side box and whisker plot using annual maximum series (AMS) of 20 global climate models (GCMs) under RCP4.5 at the Denton station compared to the historical AMS

Under the RCP8.5 scenario, two GCMs (CanESM2 and HadGEM2-CC365) had higher outlier values (> 11 inches/day) than historical AMS outliers (10 inches/day), as shown in Figure 5.

While comparing the whisker length, the majority of GCMs had higher upper whiskers suggesting that AMS values were positively skewed. In addition, the coefficient of skewness, as shown in Table 6, also showed positive values indicating right-tail skewness. Finally, while comparing the median value except for one GCM (MIROC-ESM-CHEM), all other GCMs showed AMS median values less than or equal to the historical AMS values (Table 6).

Table 6: Descriptive statistics of annual maximum series of 20 global climate modes (GCMs) under RCP8.5 at the Denton station

| GCMs	Mean	Median	Standard Deviation	Skewness Coefficient
Denton 2 SE	3.1	3.1	1.1	1.0
Bcc-csm1-1-m	3.3	3.0	1.1	0.9
Bcc-csm1-1	2.7	2.6	0.7	0.6
BNU-ESM	3.1	2.8	1.7	2.8
CanESM2	2.7	2.6	0.7	0.3
CCSM4	3.1	2.7	1.4	2.2
CNRM_CM5	3.2	2.8	1.6	2.2
CSIRO-Mk3-6-0	2.9	2.8	1.0	1.1
GFDL-ESM2G	3.0	2.6	1.7	3.2
GFDL-ESM2M	2.7	2.6	0.9	1.2
HadGEM2-CC365	3.0	2.6	1.3	1.3
HadGeM2-ES365	2.5	2.4	0.8	1.2
inmcm4	3.1	3.0	1.4	2.2
IPSL-CM5A-LR	2.6	2.3	1.2	2.8
IPSL-CM5A-MR	3.1	3.1	1.0	0.4
IPSL-CM5B-LR	2.9	2.9	0.9	1.6
MIROC-ESM-CHEM	3.4	3.3	1.1	0.5
MIROC-ESM	2.7	2.6	0.9	0.8
MIROC5	2.7	2.5	1.2	3.1
MRI-CGCM3	2.6	2.4	0.9	0.9
NorESM1-M	3.1	3.1	1.1	1.0
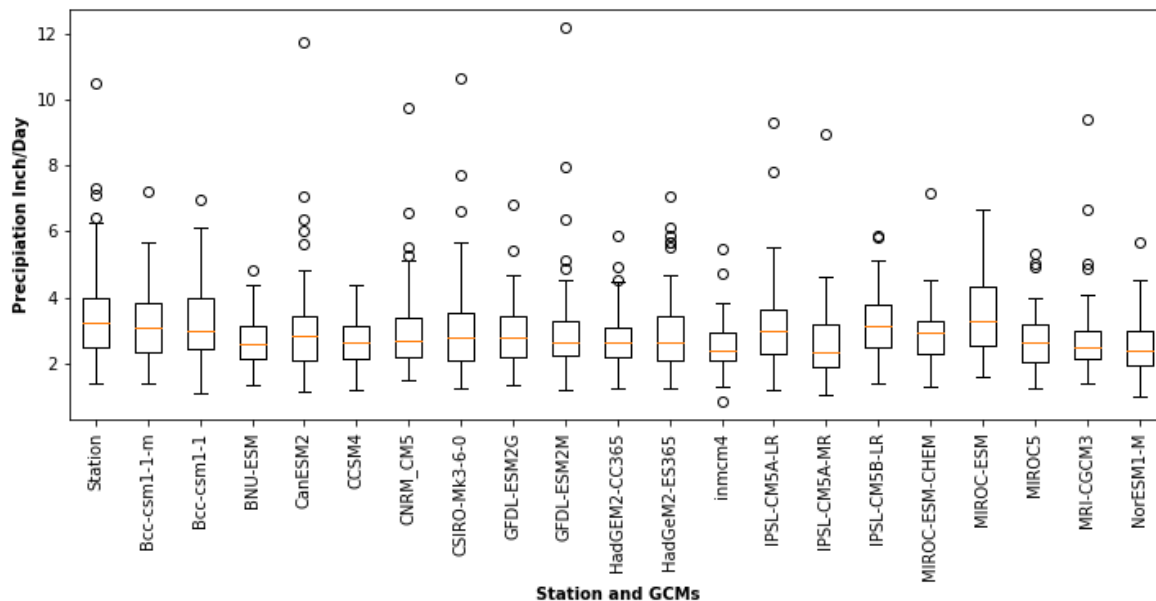
Figure 5: A side-by-side box and whisker plot using annual maximum series (AMS) of 20 global climate models (GCMs) under RCP8.5 compared to the historical AMS at the Denton station

3.2 Trend Test

Five null hypothesis significant tests were used and analyzed to identify stations with non-stationary trends in AMS over time. The results showed that out of the 88 NOAA Atlas 14 stations in the DFW metroplex, 22 stations showed a trend in at least one test (). Only one station (i.e., L.B.J National Grasslands) showed a non-stationary trend in three different tests (KPSS, ADF, and PP test). Seven stations (Corsicana, Denton 2 SE, Farmersville, Gordon 1 SW, Gunter 5 S, Morgan Mill, and Rainbow stations) showed a non-stationary trend in both MK and Pettitt tests. Fourteen stations showed a non-stationary trend in only one test, and the remaining stations showed no trend in any of the five tests. When comparing between the null hypotheses significant tests, Pettitt's test showed a trend in twelve stations, the MK test showed a trend in eight stations, the KPSS test showed non-stationarity in six stations, the ADF test

showed non-stationarity in five stations, and the PP test showed non-stationarity in one station (Table 7).

Finally, a total of seven stations (Corsicana, Denton 2 SE, Farmersville, Gordon 1 SW, Gunter 5 S, Morgan Mill, and Rainbow stations) that showed the trend in two out of five tests were selected and used for further analysis. Despite the limited number of non-stationary stations, it is important to conduct studies on these stations to understand the consequences of ignoring non-stationarity when developing IDF curves. Although the L.B.J. National Grassland station showed positive trends in three tests, it was discarded due to a lack of 30 years of continuous AMS data.

Table 7: Stations showing trends in annual maximum precipitation in a minimum of two null hypothesis significant tests and their associated p-values

Stations Name	Mann-Kendall (MK)*	Pettitt*	Kwiatkowski-Phillips-Schmidt-Shin (KPSS)*	Augmented Dickey Fuller (ADF)**	Phillips Perron (PP)**
Corsicana	0.004	0.002			
Denton 2 SE	0.018	0.001			
Farmersville	0.004	0.020			
Gordon 1 SW	0.006	0.017			
Gunter 5 s	0.029	0.024			
L.B.J National Grasslands			0.023	0.820	0.06
Morgan Mill	0.012	0.020			
Rainbow	0.012	0.020			

*Note:*p-value smaller than 0.05 indicates non-stationary trend in MK, Pettit tests and, whereas **p-value higher than 0.05 indicates non-stationary trend in ADF and PP tests.*

Similarly, while conducting trend tests for future AMS (GCMs) at Denton, the results showed that out of 20 GCMs under each RCP scenario, one GCM (IPSL-CM5A-LR) under

the RCP4.5 scenario and one GCM (HadGEM2-ES365) under RCP8.5 scenario showed positive trend tests. Hence, for these GCMs, future IDF curves were developed assuming a non-stationary trend, while for the rest of the GCMs and RCPs, future IDF curves were developed with a stationary assumption.

3.3 IDF Curves

In this study, a total of 47 IDF curves were developed. Seven non-stationary IDF curves were developed for those seven stations where historical AMS data exhibited non-stationary trends. Based on future climate, 40 IDF curves (20 GCMs X 2 RCPs) were developed for one of the representative stations (i.e., Denton).

3.3.1 Non-Stationary IDF Curves

Non-stationary assumption-based IDF curves were developed using the Pro-NEVA tool for the seven stations that showed a non-stationary trend in the trend test. When comparing IDF curves developed based on non-stationary assumption with the stationary assumption-based Atlas 14, it was found that with the stationary assumption, the rainfall intensities for all return periods (2-year, 10-year, 20-year, 50-year, and 100-year) were underestimated, as shown in Figure 6 at the Corsicana station, Figure 7 at the Denton station, Figure 8 at the Farmersville station, Figure 9 at the Gordon station, Figure 10 at the Gunter station, Figure 11 at the Morgan Hill station, and Figure 12 at the Rainbow station.

3.3.1.1 Corsicana

The 24-hour rainfall intensity of non-stationary-based IDF curves for Corsicana station (Figure 6) for 2-year, 10-year, 20-year, 50-year, and 100-year were 4.20 inches, 6.94 inches, 8.38 inches, 10.25 inches, and 11.96 inches, respectively. In comparison, stationary-based 24-hour rainfall intensities were 3.21 inches, 5.2 inches, 6.38 inches, 7.64 inches, and 8.84 inches, respectively. Regarding the percentage change between stationary and non-stationary conditions, as shown in Table 8, the 24-hour rainfall intensity increased by 30.8%, 32.7%, 33.3%, 34.2%, and 35.3% for 2-year, 10-year, 20-year, 50-year, and 100-year, respectively. It was found that there was a systematic underestimation of 24-hour precipitation intensity under the stationary condition, with higher underestimation for longer return periods by 14.6% compared to the shorter return periods.

Figure 6: Comparison between the non-stationary (red lines) and Atlas 14 (blue lines) at the Corsicana station for one-day duration IDF curves, along with 90% confidence intervals

3.3.1.2 Denton 2 SE

The 24-hour rainfall intensity of non-stationary-based IDF curves for Denton for 2-year (Figure 7), 10-year, 20-year, 50-year, and 100-year return periods were 4.20 inches, 8.35 inches, 10.28 inches, 12.65 inches, and 14.39 inches, respectively. In comparison, that of stationary-based 24-hour precipitation intensities were 3.23 inches, 5.20 inches, 6.28 inches, 7.65 inches, and 8.75 inches, respectively. Regarding percentage change between stationary and non-stationary conditions, as shown in Table 8, the 24-hour rainfall intensity increased by 29.4%, 58.1%, 63.6%, 65.4%, and 65.4% for 2-year, 10-year, 20-year, 50-year, and 100-year, respectively. It was found that there was a systematic underestimation of 24-hour precipitation intensity under the stationary condition, with higher underestimation for longer return periods by 122.45% compared to the shorter return periods.

*Figure 7: Comparison between the non-stationary (red lines)
and Atlas 14 (blue lines) at the Denton station for one day
duration IDF curves, along with 90% confidence interval*

3.3.1.3 Farmersville

The 24-hour rainfall intensity of non-stationary-based IDF curves for Farmersville (Figure 8) for 2-year, 10-year, 20-year, 50-year, and 100-year were 5.16 inches, 7.41 inches, 8.10 inches, 8.90 inches, and 9.40 inches, respectively, while the stationary-based values were

3.76 inches, 5.33 inches, 5.91 inches, 6.51 inches, and 6.99 inches, respectively. The difference between stationary and non-stationary conditions are shown in Table 8. The 24-hour rainfall intensity increased by 37.2%, 39.0%, 37.1%, 36.7%, and 34.5% for 2-year, 10-year, 20-year, 50-year, and 100-year, respectively. It was found that there was a systematic underestimation of 24-hour precipitation intensity under the stationary condition, with higher underestimation

*Figure 8: Comparison between the non-stationary (red lines)
and Atlas 14 (blue lines) at the Farmersville station for one
day duration IDF curves, along with 90% confidence
intervals*

for shorter return periods by 7.8% compared to the longer return periods.

3.3.1.4 Gordon 1 SW

The 24-hour rainfall intensity of non-stationary-based IDF curves for Gordon (Figure 9) for 2-year, 10-year, 20-year, 50-year, and 100-year were 4.99 inches, 8.97 inches, 10.48 inches, 12.32 inches, and 13.81 inches, respectively. In contrast, for the stationary-based IDF curves, the 24-hour rainfall intensities were 3.21 inches, 5.28 inches, 6.16 inches, 7.19 inches, and 8.05 inches, respectively. As shown in Table 8 , it was found that the 24-hour rainfall intensity increased by 55.5%, 69.9%, 70.1%, 71.3%, and 71.6% for 2-year, 10-year, 20-year,

50-year, and 100-year, respectively when the IDF curves were built considering non-stationary assumption as compared to the stationary assumption. It was found that there was a systematic underestimation of 24-hour precipitation intensity under the stationary condition with higher underestimation for longer return periods by 29% compared to the shorter return periods.
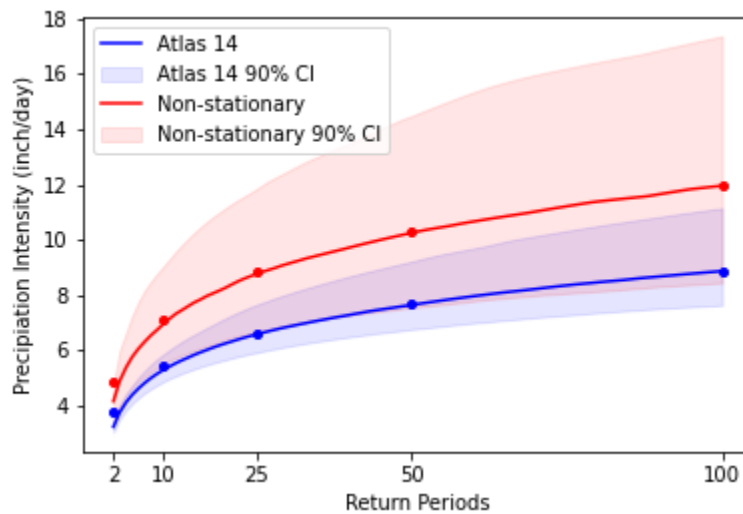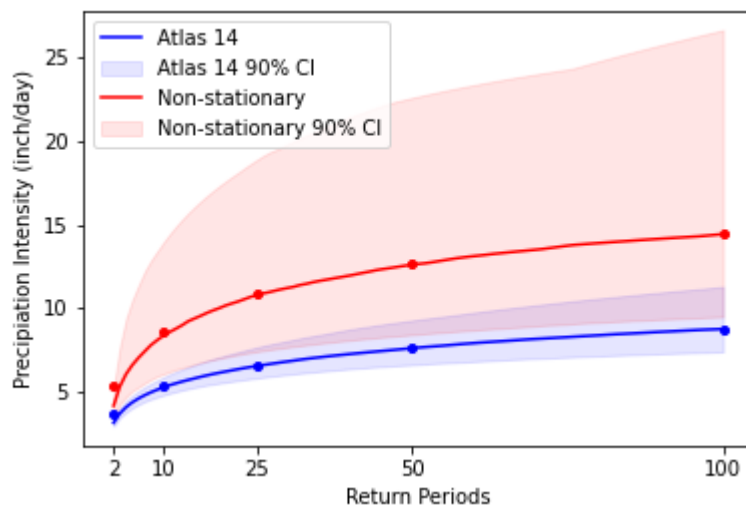

Figure 9: Comparison between the non-stationary (red lines) and Atlas 14 (blue lines) at Gordon 1 SW station for one day duration IDF curves, along with 90% confidence intervals

3.3.1.5 Gunter 5 S

The 24-hour rainfall intensity of non-stationary-based IDF curves for Gunter (Figure 10) for 2-year, 10-year, 20-year, 50-year, and 100-year return periods were 5.25 inches, 8.97 inches, 10.68 inches, 12.60 inches, and 14.35 inches, respectively, while for the stationary-based IDF curves, these values were 3.65 inches, 5.85 inches, 6.85 inches, 8.02 inches, and 8.95 inches, respectively. The comparison between the stationary and non-stationary IDF curves is shown in Table 8. The 24-hour rainfall intensity increased by 43.8%, 53.3%, 55.9%,

57.1%, and 60.3% for 2-year, 10-year, 20-year, 50-year, and 100-year return periods, respectively, under the non-stationary assumption. It was found that there was a systematic
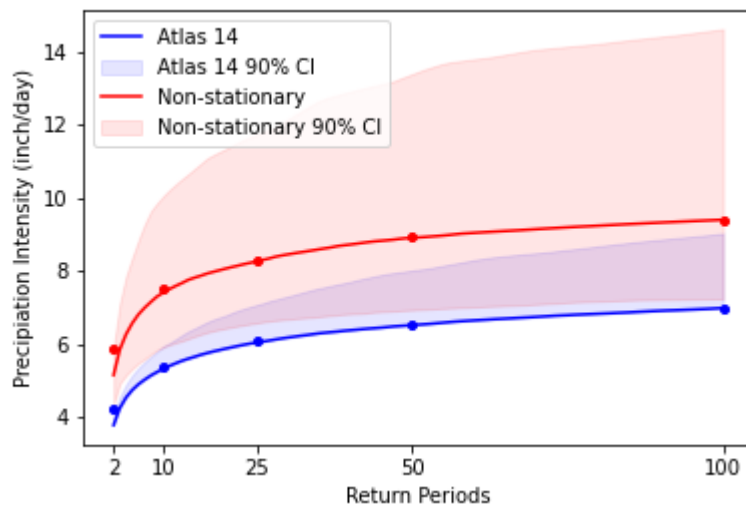

Figure 10: Comparison between the non-stationary (red lines) and Atlas 14 (blue lines) at the Gunter 5 S station for one day duration IDF curves, along with 90% confidence intervals

underestimation of 24-hour precipitation intensity under the stationary condition, with higher underestimation for longer return periods by 37.67% compared to the shorter return periods.

3.3.1.6 Morgan Mill

The 24-hour rainfall intensity of non-stationary-based IDF curves for Morgan Mill (Figure 11) for 2-year, 10-year, 20-year, 50-year, and 100-year return periods were 4.47 inches, 8.19 inches, 9.87 inches, 12.10 inches, and 13.87 inches, respectively. In comparison, the 24-hour rainfall intensity of stationary-based IDF curves for the same return periods were 3.15 inches, 5.68 inches, 6.77 inches, 8.11 inches, and 9.28 inches, respectively.

These changes between the stationary and non-stationary conditions are shown in Table 8. The 24-hour rainfall intensity increased by 41.9%, 44.2%, 45.8%, 49.2%, and 49.5% for the 2-year, 10-year, 20-year, 50-year, and 100-year, respectively, under the non-stationary assumption. It was found that there was a systematic underestimation of 24-hour precipitation intensity under
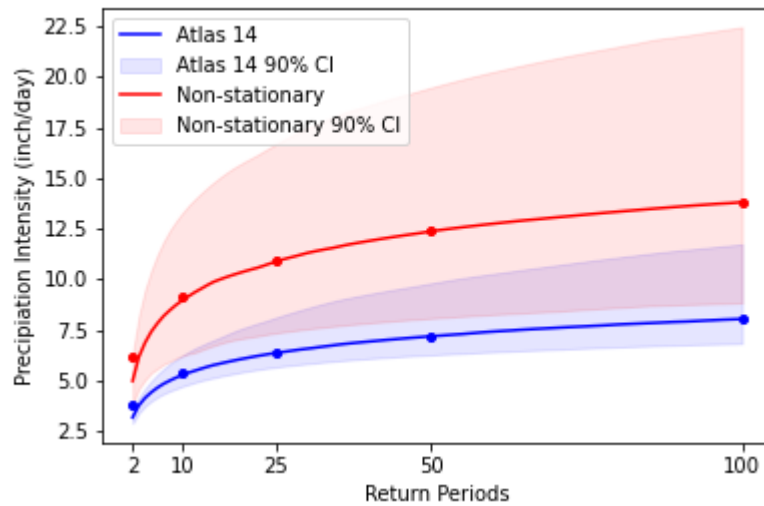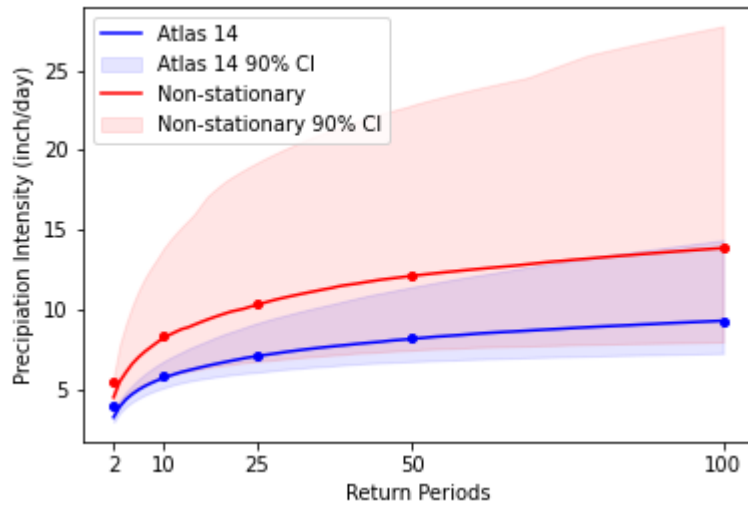
Figure 11: Comparison between the non-stationary (red lines) and Atlas 14 (blue lines) at the Morgan Mill station for one day duration IDF curves, along with 90% confidence intervals

the stationary condition, with higher underestimation for longer return periods by 18% compared to the shorter return periods.

Table 8: Difference between Atlas 14 (stationary) and non-stationary 24-hour precipitation intensities for five return periods at seven stations in the Dallas-Fort Worth metroplex

Stations	Percentage change (%) one-day precipitation intensities at five return levels				
	2-Year	10-year	20-year	50-year	100-year
Corsicana	30.8	32.7	33.3	34.2	35.3
Denton 2 SE	29.4	58.1	63.6	65.4	65.4
Farmerville	37.2	39	37.1	36.7	34.5
Gordon 1 SW	55.52	69.9	70.1	71.3	71.6
Gunter 5 S	43.8	53.3	55.9	57.1	60.3
Morgan Mill	41.9	44.2	45.8	49.2	49.5
Rainbow	33.7	58.9	65.5	71.9	74.3

3.3.1.7 Rainbow

The 24-hour rainfall intensity of non-stationary-based IDF curves for Rainbow (Figure 12) for return periods of 2-year, 10-year, 20-year, 50-year, and 100-year were 4.01 inches, 7.80 inches, 9.65 inches, 11.93 inches, and 13.77 inches, respectively. In comparison, the 24-hour rainfall intensity of stationary-based IDF curves for the same return periods were 3.0 inches, 4.91 inches, 5.83 inches, 6.94 inches, and 7.90 inches, respectively. These changes are shown in Table 8. The 24-hour rainfall intensity increased by 33.7%, 58.9%, 65.5%, 71.9%, and
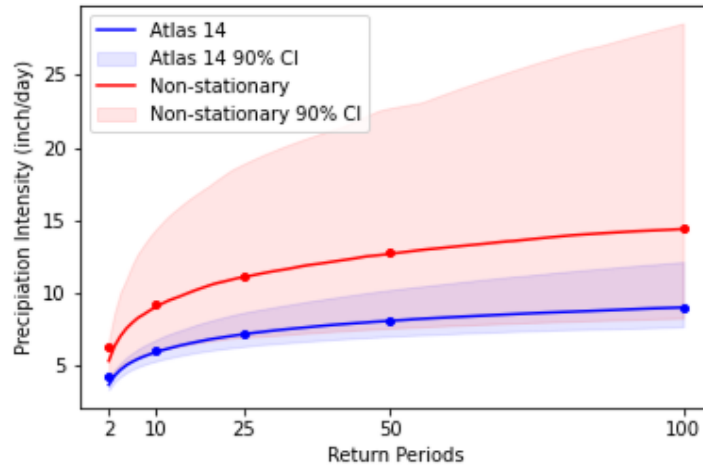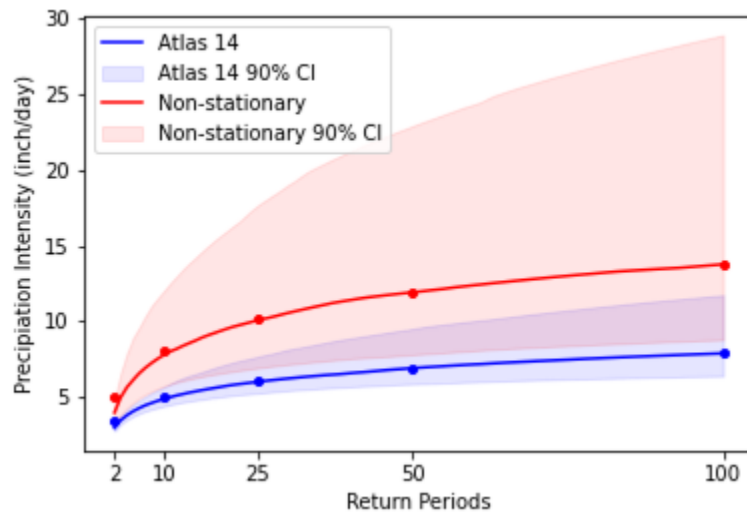

Figure 12: Comparison between the non-stationary (red lines) and Atlas 14 (blue lines) at the Rainbow station for one day duration IDF curves, along with 90% confidence intervals

74.3% for 2-year, 10-year, 20-year, 50-year, and 100-year return periods, respectively, under the non-stationary assumption. In addition, it was found that there was a systematic underestimation of 24-hour precipitation intensity under the stationary condition with higher underestimation for longer return periods by 120% compared to the shorter return periods.

3.3.2 Future IDF Curves

Future precipitation IDF curves were developed for Denton using projections from 20 GCMs under RCP4.5 and RCP8.5. For each RCP scenario, 19 IDF curves were developed

based on the stationary assumption. In contrast, one IDF curve was developed for each RCP based on the non-stationary assumption as per the trend test result. Therefore, out of 40 combinations of GCMs and RCPs, two GCMs showing non-stationary trends (IPSL-CM5A-LR under RCP4.5 and HadGEM2-ES365 under RCP8.5) were used to develop non-stationary IDF curves. For the remaining 38 GCMs, stationary IDF curves were built.

3.3.2.1 Future IDFs under GCMs with RCP8.5

Differences between Atlas 14 and GCM RCP8.5-based 24-hour precipitation intensities for five return periods (2-year, 10-year, 25-year, 50-year, and 100-year) are reported in Table 9. The results showed noticeable differences in extreme precipitation events across GCMs and return periods. Overall, there would be a decrease in 24-hour precipitation intensities in 19 GCMs developed based on stationary assumption, ranging from 1.5% to 49.1%. The most significant changes were found in the higher return periods (i.e., 50-year and 100-year), with one GCM showing reductions as high as 49%, while rest of the 14 GCMs showed reduction >24% in 24-hour precipitation intensity for the 100-year return period. Four GCMs (CCSM4, BNU-ESM, inmcm4, and NorESM1-M) showed a substantial decrease in precipitation intensity across all return periods; however, the reduction for the 100-year return period was 40% or larger (Table 9 and Figure 13). On the contrary, one GCM HadGEM2-ES365, developed based on non-stationary assumption, showed a wide range of increase of 24-hour precipitation intensity in all return periods, whereas two GCMs CSIRO-Mk3-6-0 and MIROC-ESM developed based on stationary assumption indicated increases in a specific return period (Table 9). For HadGEM2-ES365, the 24-hour precipitation intensity increased in all return periods ranging from 18% to 32.0%. The highest increase (32.0%) was found in the 25-year return period, followed by a 31.9% increase for the 100-year return period, with the

Figure 13: Percentage change calculated between Atlas 14 and GCMs' 24-hour duration, 100-year intensity-duration-frequency curves of the Denton station under RCP8.5

lowest increase of 18.0% found in the 2-year return period, as shown in Table 9.CSIRO-Mk3-6-0 showed an increase in the 24-hour precipitation intensity in the 100-year return period by 2.3%, with virtually no change (0.01%) in the 50-year return period. For MIROC-ESM, the 24-hour precipitation intensity increased the most (4.3%) in the 2-year return period. Similarly, other GCMs (e.g., CanESM2, CNRM_CM5, GFDL-ESM2M, and IPSL-CM5A-MR) exhibited higher reductions in the 24-hour precipitation intensity in lower return periods compared to 50-year and 100-year return periods (Table 9). Among all GCMs, IPSL-CM5A-MR showed the highest reduction of 25.0% in 2-year return periods.

Table 9: Differences between Atlas 14 and future climate-based 24-hour precipitation intensities at the Denton station for five return periods

GCMS under RCP8.5	Percentage change (%) at five return levels				
	2-year	10-year	25-year	50-year	100-Year
Bcc-csm1-1	-1.6	-9.3	-15.3	-19.8	-24.3
Bcc-csm1-1-m	-5.9	-12.1	-16.9	-21.0	-24.8
BNU-ESM	-18.2	-30.5	-36.4	-40.9	-44.9
CanESM2	-14.2	-6.9	-4.5	-3.2	-1.9
CCSM4	-16.2	-30.8	-38.5	-44.1	-49.1
CNRM_CM5	-13.0	-10.7	-8.4	-6.1	-3.1
CSIRO-Mk3-6-0	-9.9	-4.2	-1.5	0.0	2.3
GFDL-ESM2M	-14.9	-8.9	-5.9	-4.7	-3.2
GFDL-ESM2G	-13.1	-18.1	-21.9	-25.1	-28.4
HadGEM2-CC365	-17.5	-26.2	-30.6	-34.0	-37.1
HadGEM2-ES365	18.0	31.0	32.0	31.7	31.9
inmcm4	-23.6	-32.5	-37.8	-41.6	-45.5
IPSL-CM5A-LR	-9.4	-9.8	-10.8	-12.3	-13.4
IPSL-CM5A-MR	-25.3	-24.2	-24.0	-24.3	-24.3
IPSL-CM5B-LR	-2.8	-13.0	-20.4	-26.4	-31.7
MIROC5	-19.2	-26.4	-31.5	-35.6	-39.3
MIROC-ESM	4.3	-6.1	-13.5	-19.4	-24.9
MIROC-ESM-CHEM	-12.9	-21.5	-26.1	-30.0	-33.6
MRI-CGCM3	-21.6	-24.2	-24.4	-24.8	-24.8
NorESM1-M	-23.0	-28.5	-32.9	-36.6	-40.0

3.3.2.2. Future IDFs with GCMs under RCP4.5

Any differences in the 24-hour precipitation intensity as expressed in percentage change between Atlas 14 and GCMs under the RCP4.5 scenario for five different return periods (2-year, 10-year, 25-year, 50-year, and 100-year) are reported in Table 10. Overall, the results showed a decrease in the 24-hour precipitation intensity in 19 GCMs, ranging from 1.8% to

41.5%, which are developed based on stationary assumption. The largest changes were found in the higher return periods (50-year and 100-year), with one GCM (MRI-CGCM3) showing reductions up to 41.5% in the 24-hour precipitation intensity for the 100-year return period. In addition, five GCMs (MRI-CGCM3, NorESM1-M, MIROC-ESM-CHEM, Bcc-csm1-1-m, and BNU-ESM) showed a marked decrease in the 24-hour precipitation intensity across all return periods. However, for the 100-year return period, the reduction was greater than 30% (Figure 14).
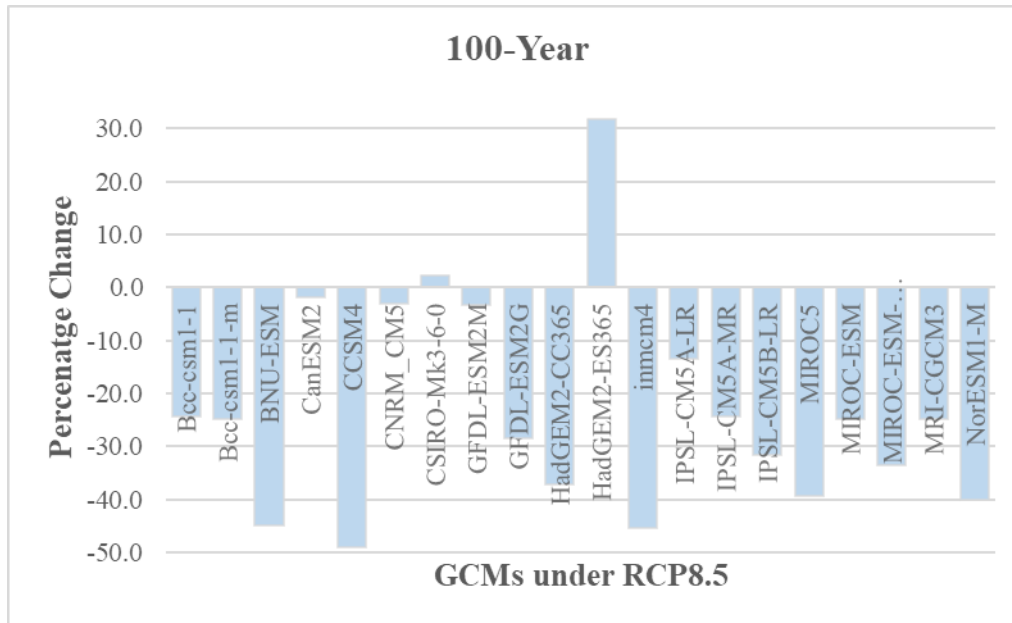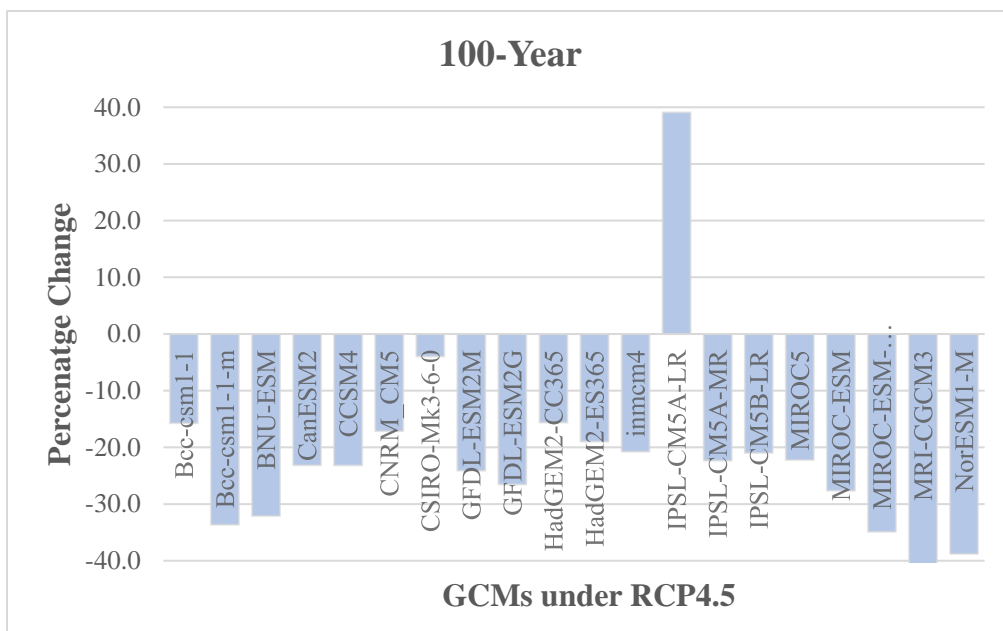

Figure 14: Percentage change calculated between Atlas 14 and GCMs 24-hours duration, 100-year Intensity Duration Frequency (IDF) curves at the Denton station under RCP4.5

On the contrary, one GCM (IPSL-CM5A-LR) showed an increase in the 24-hour precipitation intensity in all return periods, which was developed based on non-stationary assumption, with the lowest increase of 21.0% in the 2-year return period and the highest increase of 39.0% in the 100-year return period. Table 10 showed that 15 GCMs had the largest impact in longer return periods (50-year and 100-year). Three GCMs (CSIRO-Mk3-6-0, CanESM2, and HadGEM2-ES365) showed the largest effect in lower return periods (2 to 25-year), whereas

only one GCM (HadGEM2-CC365) indicated the largest impact (-18.7%) in the 10-year

increased form 2 years (-14.7%) and slowly decrease towards100-years and ended up at 15.6%

reduction. Among all GCMs, a large decrease in 2-years, 10-year, 25-year, and 50-year was

seen in NorESM1-M, i.e., 25.2%, 29.3%, 32.8%, and 35.8%, respectively, whereas the highest

reduction (41.5%) in 100-year return period was seen in MRI-CGCM3.

Table 10: Differences between Atlas 14 and future climate-based 24-hour precipitation intensities for five return periods at the Denton station

GCMs under RCP4.5	Percentage change (%) at five return levels				
	2-year	**10-year**	**25-year**	**50-year**	**100-Year**
Bcc-csm1-1	-7.0	-10.3	-11.9	-13.8	-15.7
Bcc-csm1-1-m	-15.5	-22.8	-26.9	-30.4	-33.7
BNU-ESM	-15.0	-21.8	-25.9	-29.2	-32.1
CanESM2	-23.6	-23.6	-23.4	-23.3	-23.2
CCSM4	-18.2	-20.2	-21.4	-22.2	-23.2
CNRM_CM5	-17.1	-15.2	-15.6	-16.3	-17.2
CSIRO-Mk3-6-0	-5.7	-4.3	-3.8	-3.8	-4.0
GFDL-ESM2M	-16.1	-16.5	-19.1	-21.8	-24.1
GFDL-ESM2G	-10.7	-14.4	-18.7	-22.9	-26.5
HadGEM2-CC365	-14.7	-18.7	-17.8	-16.8	-15.6
HadGEM2-ES365	-22.9	-23.8	-22.5	-20.8	-19.0
inmcm4	-13.3	-15.1	-17.1	-18.8	-20.7
IPSL-CM5A-LR	21.1	30.9	31.6	35.6	39.1
IPSL-CM5A-MR	-16.3	-15.8	-18.2	-20.4	-22.3
IPSL-CM5B-LR	-4.5	-10.2	-14.6	-17.9	-21.0
MIROC5	-18.5	-21.8	-22.1	-22.4	-22.2
MIROC-ESM	-1.8	-11.8	-17.9	-23.0	-27.6
MIROC-ESM-CHEM	-14.9	-22.6	-27.3	-31.3	-34.9
MRI-CGCM3	-7.5	-21.6	-29.7	-35.7	-41.5
NorESM1-M	-25.2	-29.3	-32.8	-35.8	-38.8

3.3.3 Non-Stationary IDF Curves Comparison

For the Denton station, three non-stationary IDF curves were developed (Figure 15). One was based on the historical precipitation and the other on GCMs under each RCP scenario. For RCP4.5 and RCP8.5, projections from IPSL-CM5A-LR and HadGEM2-ES365 were used, respectively. While comparing three non-stationary IDF curves, it was found that the 24-hour
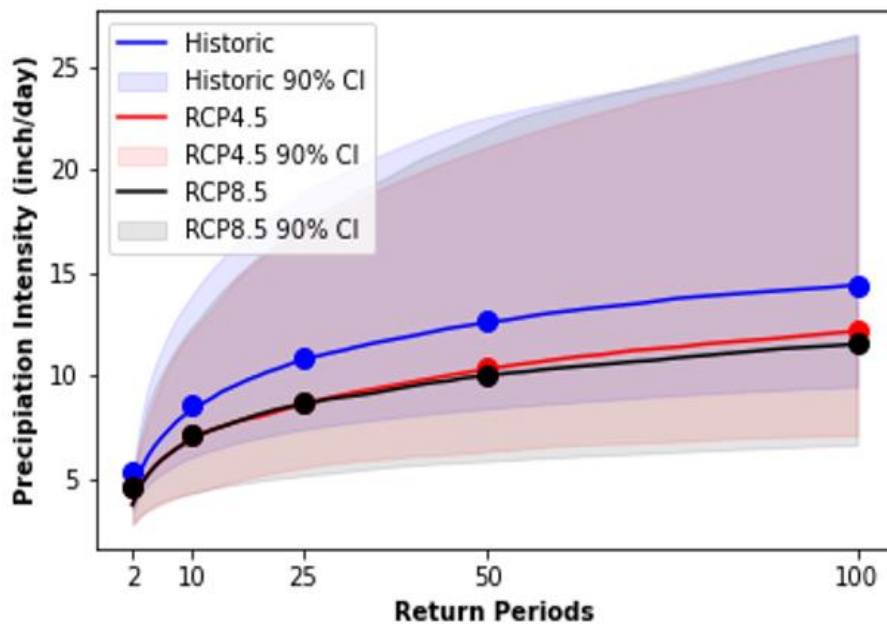
Figure 15: Non-stationary IDF curve based on historical and future precipitation data (under RCP4.5 and RCP8.5 scenarios) with their 90% confidence intervals

precipitation intensities in all return periods were high in the case of historical non-stationary IDF curves compared to the future. It implies that consideration of non-stationarity in IDF curve development could be sufficient to cover future climatic conditions. It is because projected GCM ensembles showed a decline in extreme precipitation events in the DFW metroplex compared to the historical AMS.

3.3.4. Stationary and Non-Stationary Model Comparison

Based on the Table 11, the non-stationary model performed better than the stationary model for most of the stations. As indicated by the lower values of Akaike information criterion

(AIC), Bayesian information criterion (BIC), and root mean square error (RMSE), as well as the higher values of Nash-Sutcliffe model efficiency coefficient (NSE), for the non-stationary model compared to the stationary model (Table 11), non-stationary models seemed to perform well for majority of the stations. While comparing AIC value, non-stationary model showed lower value for all seven stations indicating they are better fit. However, in case of BIC, RMSE and NSE non-stationary models seem to provide better fits at majority of the stations.

Table 11: Goodness of fit statistics of stationary and non-stationary models for seven stations

Stations	Model	Akaike information criterion (AIC)	Bayesian information criterion (BIC)	Root mean square error (RMSE)	Nash-Sutcliffe model efficiency coefficient (NSE)
Corsicana	Stationary	359.42	367.66	3.15	0.95
	Non-Stationary	355.62	369.35	2.44	0.97
Denton	Stationary	329.00	336.85	1.71	0.98
	Non-Stationary	325.91	338.99	1.41	0.99
Farmersville	Stationary	151.55	157.41	1.52	0.97
	Non-Stationary	146.95	156.70	1.58	0.97
Gordon	Stationary	221.14	227.71	1.41	0.98
	Non-Stationary	216.36	227.31	1.72	0.97
Gunter	Stationary	179.73	185.53	2.38	0.94
	Non-Stationary	178.63	188.29	2.79	0.92
Morgan Mill	Stationary	210.16	216.34	1.61	0.97
	Non-Stationary	210.01	220.31	2.37	0.95
Rainbow	Stationary	235.50	242.53	1.85	0.97
	Non-Stationary	231.93	243.65	1.53	0.98

Chapter 4: Discussions

In this research project, differences between the 24-hour precipitation intensity as observed in the historical precipitation and stationary-based IDF curves (Atlas 14) and future climate and non-stationary-based IDF curves were investigated for the fourth largest metropolitan region (DFW metroplex) in the U.S. with an urban population of nearly eight million and growing. Using the widely accepted and recommended scientific and statistical methods, this study found that 25% of the Atlas 14 stations in the DFW metroplex exhibited non-stationary trends with time in at least one out of five tests as opposed to the Atlas 14 assumption. Among the five tests, 13%, 9%, 7%, 6%, and 1% stations showed a non-stationary trend for Petitt, MK, KPSS, ADF, and PP tests, respectively. In statistical literature about time series data, usually, three tests (KPSS, ADF, and PP) are considered direct tests for non-stationarity testing; however, their results sometimes disagree (Afriyie et al., 2020), similar to what was found in this study. Except for one out of 88 stations, the KPSS, ADF, and PP tests results were in disagreement. Such a disagreement and reduced test accuracy could be attributed to the sample size used in the trend detection test agreement, and accuracy among the tests generally improves with increasing sample sizes (Liu et al., 2022). The other two tests (MK and Pettitt tests) applicable for trend detection are popularly used and recommended in hydrology and climate literature (Cheng et al., 2014; Sam et al., 2022; Um et al., 2018) for analyzing hydro-climatological time series data including precipitation AMS (Perica et al., 2018). The Pettitt test detects abrupt changes in AMS data (Conte et al., 2019; Rougé et al., 2013) and is a robust method for trend detection. Therefore, in addition to the Pettitt test, the MK test, also adopted by Atlas 14, was used in this research project to determine the presence of a non-stationarity trend in the precipitation AMS data for historical and future periods. The

majority (75%) of the stations in this study showed stationary trends with time. However, neglecting the non-stationarity characteristics of the remaining stations to assess risks associated with extreme events, especially in the face of rapidly changing climatic conditions, may prove costly to coupled human-natural systems (Markolf et al., 2021; Ren et al., 2019). For instance, Underwood et al. (2017) stated that changing climate will add roughly $22 to $36 billion in transportation and other infrastructure costs related to pavement maintenance and new construction in the U.S. by 2070. Further, required mitigation measures and damages associated with climate change are often exacerbated by growing and unsustainable urban growth; therefore, assessment studies should not discount low-probability events (Chen et al., 2021; Sterzel et al., 2020; Zhou et al., 2019).

It is quite difficult to pinpoint reasons for these 7 stations (Corsicana, Denton 2 SE, Farmersville, Gordon 1 SW, Gunter 5 S, Morgan Mill, and Rainbow (Figure 1 and Table 5) for showing non-stationary trend without further research. However, some potential reasons related to stations' locations, physical environments, landforms, vegetation, and rural-urban fringe creating unique microclimates might offer some insights. The Corsicana station, located in the southeastern side of the DFW metroplex, displayed non-stationarity. One potential reason for this trend could be a normally increasing west-east precipitation gradient in Texas and the U.S. (Easterling et al., 2017). Moreover, Corsicana is located in a low-lying area with numerous creeks and streams, and is surrounded by larger water bodies such as Richland-Chambers Reservoir, Navarro Mills Lake, and Lake Bardwell (Cox, 2006; NCTCOG, 2015). These water bodies along with varied landscapes could have potentially created a microclimate contributing to the non-stationary trend. However, other nearby stations with the presence of water bodies in their periphery, did not display non-stationary trend, indicating the influence

of other factors. One such factor could be the highly urbanized location of Corsicana. According to Liu & Niyogi (2019), urbanization modifies rainfall amount and intensity within different areas of a city, resulting in an increase in mean precipitation downwind of the city by 18%, over the city by 16%, and on the left and right of the city by 2% and 4%, respectively. Potential changes in rainfall patterns in urban areas (Patra et al., 2018) could be attributed to the interaction of factors such as aerosol emissions, surface roughness, and heat storage Song et al., (2021).

The Denton station is situated in an urbanized area in close proximity to Lewisville Lake. Additionally, it has diverse topography with rolling hills. When compared to nearby stations that are located closer to Lewisville Lake (Figure 1), Denton station exhibits a distinctive non-stationary trend in the AMS data. Most likely, local topography, large lake effect and its urban growth could be potential contributing factors to the observed non-stationary trend. Some studies suggest that location-specific topography and slopes which alter humidity and wind motion and direction could affect local extreme precipitation variability (Li & Hu, 2019; Zhao et al., 2020).

The stations of Gordon 1 SW, Rainbow, and Morgan Mill are situated in southwestern DFW. Adjacent to these stations on western side, there are mountains (Clayton and Palo Pinto Mountains), and on eastern side, there are a number of streams and lakes, which may have added orographic effects and caused erratic and higher precipitation events (Marra et al., 2022). The Gordon station, which is located closer to the mountain, has a higher AMS value followed by Morgan Mill and Rainbow stations (Figure 3), which are situated farther away from the mountains (Figure 1). Additionally, these stations are located near highways and urbanized areas, much like the Denton and Corsicana stations.

Furthermore, issues related to screening and quality control (correction of missing, underestimated, or erroneously recorded events) of the AMS data by NOAA (Perica et al., 2018) could also be a potential factor. NOAA used a combination of data sources (nearby gauges, storm reports, storm data, and radar data) to determine unconstrained 24-hour annual maximum values for extreme events. Therefore, trend tests (stationary or non-stationary) may subject to data mining and quality control methods.

The development of IDF curves for seven out of 88 stations exhibiting non-stationarity indicated substantially higher (up to 75%) 24-hour precipitation intensities for five return periods (2-year, 10-year, 20-year, 50-year, and 100-year) compared to the Atlas 14 that assumed stationarity of precipitation AMS with time (Table 8). While the benchmark 100-year return period showed an increase of 34.5 to 74.3%, the most frequently occurring 2-year storm event indicated an increase of up to 55% compared to the Atlas 14. These findings in the DFW metroplex are consistent with studies done in other metropolitan regions in the U.S. and elsewhere. For example, a study conducted by Cheng & Aghakouchak (2015) at White Sands National Monument Station, New Mexico, found that non-stationary IDF curves produced higher rainfall intensities than stationary IDF curves. The authors observed that the stationary assumption underestimated extreme precipitation as much as 60% in 2 hours duration, 2-year return period rainfall, which has the potential to increase the frequency of flood risks and infrastructure failure several folds. Another study conducted by Soumya et al. (2020) in Kerala, India, found that non-stationary IDF curves had higher rainfall intensities than stationary IDF curves, with an increase in rainfall intensity of greater than 50% for the 100-year return period under non-stationary assumption compared to that of the stationary assumption. Similarly, the study conducted in the metropolitan region of Ontario, Canada,

revealed similar findings. The authors found that for the return period of 50-100 years, the standard stationary-based IDF curves needed to be updated by 2 to 44% to reflect the increases associated with the non-stationary-based IDF curves (Ganguli & Coulibaly, 2017).

All studies mentioned above in different parts of the globe, and the results of this research in the DFW metroplex confirmed the underestimation of precipitation intensities under the business-as-usual assumption of stationary rainfall over time. The consequences of this kind of underestimation are quite severe if there were to strike storm events of increased intensities for a given return period when most of the infrastructures are designed based on traditional, stationary IDF curves (Armal et al., 2020; Hsiang et al., 2017; Masson-Delmotte et al., 2021; Miro et al., 2021; Moss et al., 2017). While globally assessing the economic damage due to climate change, Hsiang et al. (2017) state that by the end of the 21st century, the poorest third of countries are projected to experience damages between 2 and 20% of county income under RCP8.5 scenarios. Similarly, Armal et al. (2020) modeled >40% increase in average economic flood damage through the year 2050 under changing climatic conditions in the U.S.

While comparing between stations, for the 100-year return period 24-hour precipitation intensity in the DFW metroplex, the greatest change was found in Rainbow station (74%) (Table 8 and Figure 12), followed by Gordon stations (72%) and Gunter stations (60%). For the 2-year return period, the biggest change was found in Gordon (55%) (Figure 9), followed by Gunter (44%) (Figure 10) and Morgan (42%) (Figure 11). While the Corsicana station (Figure 6) showed the lowest percentage change in rainfall intensity for both 2-year (30%) and 100-year (35%) return periods. These differences across stations in the DFW metroplex could be attributed to factors related to differences in the local or microclimate, land uses, and topographic variations (Silva et al., 2021). Therefore, developing IDF curves at multiple

locations/stations with varying conditions could offer better insights to urban planners in terms of potential changes in precipitation intensities under different return periods.

While incorporating non-stationary assumptions in the IDF curve development provides benefits, some limitations should be considered. First, considering non-stationary assumptions require more complex statistical approaches and modeling techniques than including stationary assumptions. Moreover, non-stationary assumptions may produce results with higher uncertainties when including GCM-based future climate scenarios with inherent GCM-specific and resolution-related uncertainties (Agilan & Umamahesh, 2018; Ragno et al., 2018; Silva et al., 2021). In contrast, stationary assumptions are more straightforward to apply than non-stationary assumptions mainly because they do not need to account for changes in climate and weather patterns over time. Therefore, stationary assumptions may be appropriate in those cases limited by data availability and with evidence of no long-term climate change (Chandra et al., 2015). Unfortunately, the cost of stationarity assumptions could be quite high and burdensome as stationary IDF curves could lead to inaccurate estimates of extreme rainfall events in areas prone to long-term climate change, land-use change, and other meteorological factors (Singh et al., 2020). Therefore, it is crucial to detect a trend in precipitation over time and space and consider local factors before deciding on the appropriate method for the IDF curve development.

While time could be one of the covariates in the development of non-stationary IDF curves, as done in several other studies (Agilan & Umamahesh, 2017a, 2017b; Ouarda et al., 2019) and this study, it is not free of important limitations. First, time as a covariate alone may not adequately capture the complex changes in meteorological, hydrological, and environmental factors that can affect the intensity and frequency of extreme rainfall events

(Agilan & Umamahesh, 2017c). Second, the precipitation time series data may only sometimes have sufficient resolution to capture the fine-scale variations in extreme rainfall events (Rajendran et al., 2019). Third, changes in the urban and suburban landscape, such as land use and land cover changes with varying intensity of growth from mixed-use development to single-family homes to different sizes of open spaces, can affect the intensity and frequency of extreme rainfall events but cannot be adequately captured by time alone (Singh et al., 2020). Fourth, the limited data availability (e.g., lack of continuous hourly, sub-daily, and daily precipitation data for several decades) can pose a challenge in estimating the non-stationary IDF curves using only time as a covariate (Chandra et al., 2015). However, the limitation of using only time as a covariate can be addressed by using other essential covariates, such as temperature, humidity, greenhouse gases concentrations, urban extent, and ocean-atmosphere oscillations, among others. Including these covariates could improve the accuracy of estimating intensity and frequency of extreme rainfall events. Among these covariates, temperature is a crucial factor that can affect the amount and intensity of extreme rainfall events. Warmer temperatures can increase the moisture-holding capacity of the atmosphere, leading to more intense rainfall events. Studies have demonstrated that incorporating temperature into non-stationary IDF curve development can improve the accuracy of estimates for extreme rainfall events (Agilan & Umamahesh, 2017c; Roderick et al., 2020). Another covariate that can significantly impact the intensity and frequency of extreme rainfall events is topography. Steep slopes may experience more intense rainfall events due to increased convergence of airflow and uplift. In contrast, flat terrain may experience more frequent but less intense rainfall events due to slow runoff and longer residence time of water in the soil (Roderick et al., 2020). Incorporating land use and land cover changes, such as urbanization or

53

deforestation, into non-stationary IDF curve development can also help account for differences in surface properties, such as the albedo effect, that can affect the intensity and frequency of extreme rainfall events (Agilan & Umamahesh, 2017c; Singh et al., 2020). Also, large-scale atmospheric circulation patterns, such as El Niño-Southern Oscillation (ENSO) or North Atlantic Oscillation (NAO), can influence the intensity and frequency of extreme rainfall events. Incorporating these patterns into non-stationary IDF curve development can help capture the effects of climate variability and improve estimates for extreme rainfall events (Sun et al., 2017; Whan & Zwiers, 2017). The use of the aforementioned covariates, along with time, can improve the accuracy of non-stationary IDF curve development and help prepare planners for extreme events in rapidly growing and larger metropolitan areas like the DFW metroplex.

This research project also included the potential impact of incorporating GCM-based projected precipitation in IDF development for one of the DFW locations, Denton, which exhibited non-stationarity for the historical precipitation AMS and is one of the fastest-growing and rainfall-intensive regions. At Denton, GCM-based IDF curves generated mixed results showing reductions (up to 49%) in the 24-hour precipitation intensity regardless of return period in 38 (developed based on stationary assumption) out of 40 realizations of GCMs and RCPs. Two future realizations (HadGEM2-ES365 under RCP8.5 and IPSL-CM5A-LR under RCP4.5), which were developed based on non-stationary assumption (Figure 15), indicated up to 40% increase in the 24-hour precipitation intensity for the 100-year return period, which may have significant implications for water management and infrastructure planning in the rapidly growing DFW region. This result from two GCMs agrees with a study in New York, U.S., where extreme precipitation intensity was found to increase by 20-30% by the end of the century (DeGaetano & Castellano, 2017). Similarly, Ragno et al. (2018) found that in the

future, most populated U.S. cities may experience extreme precipitation intensity events up to 20% more intense and twice as frequent. Changes in the intensity of extreme precipitation under RCP8.5 was found to be more pronounced than that of RCP4.5 in Denton, as consistent with other studies in other places (AghaKouchak et al., 2018). This study found that the climatic condition in the DFW metroplex would be much drier than historically observed because even non-stationary GCMs IDF curves showed lower precipitation intensities in all return periods than non-stationary historical IDF curves. One could cautiously interpret this result as a potential reduction in the frequency and intensity of extreme precipitation or flood events in the future. However, it could also be interpreted as a higher likelihood of getting drought conditions leading to water scarcity in the region, as discussed in the Texas water plan for the next 50 years (Runkle et al., 2022; Texas Water Development Board, 2022).

The GCM-based IDF curves presented in the study should be interpreted cautiously as climate change projections have limitations related to the choice of GCMs and their coarse resolutions and methods of downscaling (statistical vs. dynamic) and bias corrections. This study used projections from 20 GCMs under two RCPs (4.5 and 8.5) from the MACA climatology lab, which used the statistical downscaling method called constructed analogs (CA) to generate 4 km resolution climate projections for the U.S. that include the study area of DFW metroplex. One of the disadvantages of the CA method is that it may only capture some of the critical spatial and temporal variability in the climate system, particularly in regions with complex topography or other local factors that can influence the climate. This limitation could lead to biased projections with poor representation of the full range of possible climate variability (Wood et al., 2002). In addition, the CA method relies on the availability and quality of historical observations, and in regions with limited data, the downscaled

projections may be less reliable (Abatzoglou & Brown, 2012). Therefore, applying other bias correction methods such as Bias Correction and Spatial Disaggregation (Thrasher et al., 2022), Machine Learning-Based Downscaling (Lezama Valdes et al., 2021), Dynamic Downscaling (Xu et al., 2021), or in some cases, combining different downscaling methods or using an ensemble of downscaled projections (Hashmi et al., 2013; Wootten et al., 2017) may provide a more robust estimate of future climate conditions. Also, the MACA projections are grid-based (4km resolution). As a result, generating a station or point-based precipitation data from the grid-based ensemble could potentially smooth peaks (e.g., daily peak rainfall amounts) (Abatzoglou & Brown, 2012). Thus, such projections may not provide accurate extreme events and cascade uncertainties in IDF curves (Lopez-Cantu et al., 2020; Noto et al., 2023). In addition, MACA GCMs under Coupled Model Intercomparison Project Phase- 5 (CMIP5) were used. However the use of the latest climate projectionsCMIP-6 might offer different future climatic conditions for the DFW region.

The DFW metroplex is in a region prone to frequent severe thunderstorms and flash floods, with many communities and infrastructure systems vulnerable to these extreme events. Using non-stationary IDF curves could capture local events and effects, making it possible to estimate the probability of extreme events in a changing climate (Silva et al., 2021). Climate change-informed IDF curves may help planners prepare for extreme events by identifying areas and infrastructure systems vulnerable to flooding and developing mitigation measures and resilient systems such as flood control systems and early warning systems. For example, non-stationary IDF curves can help identify areas likely to experience increased flooding due to climate change and assist in planning infrastructure improvements, such as drainage systems and stormwater management facilities, thereby reducing flood risks (Villarini et al., 2018).

Overall, non-stationary IDF curves can provide valuable information to planners in metropolitan areas like DFW, helping them to better prepare for and respond to extreme rainfall events. However, although these research findings are consistent with several studies conducted in different regions, caution should be exercised when interpreting these results. It is recommended that further research, particularly the use of other covariates and the use of the recently released CMIP-6 climate projections with robust downscaling and bias correction methods, be used to understand better the implications of these findings for flood risk management in the DFW metroplex.

Chapter 5: Conclusion

The frequency, severity, and randomness of precipitation extremes have generally increased over the last century worldwide, as evidenced by the growing number of flood events and billion-dollar disasters. Moreover, such precipitation-related extreme events are projected to intensify over the next several decades, risking the functioning of natural systems, increasing human casualties, and accruing unprecedented economic losses. Therefore, researchers and practitioners underscore the development and use of tools backed by science that are adaptive to such extreme events to avoid or at least decrease the associated impacts and damages to human and natural systems. For example, the IDF curve is one of the tools used to estimate potential flood risks and used as a reference in infrastructure design in many countries, including the U.S. However, like many other countries, historical precipitation records are the primary and only input to create IDF curves in the U.S.

Moreover, the historical precipitation over time is considered stationary in the existing Atlas 14. Therefore, the existing IDF curves, which designers, planners, and engineers depend on for infrastructure design in the U.S., particularly in urban areas, may not adequately capture time and space-specific climate dynamics using only historical data, which is assumed to be stationary. Therefore, this study aimed to develop IDF curves for one of the U.S.'s largest and fastest-growing metropolitan regions, the DFW metroplex, by incorporating non-stationary assumptions and future projected GCM precipitation ensembles. The results were then compared with Atlas 14, the business-as-usual tool, to quantify potential changes, if any.

First, five non-hypothesis significant tests were carried out to detect the presence of any non-stationary trend on historical AMS data using time as a covariate. The results indicated that 25% of the historical precipitation stations used in Atlas 14 in the DFW metroplex

exhibited non-stationary trends contrary to the Atlas 14 assumption. Consequently, IDF curves developed in this study using historical AMS, assuming non-stationary precipitation with time, indicated that the 24-hour precipitation intensity would increase in all seven stations in all return periods. One station showed up to a 75% increase in 24-hour precipitation intensities in a 100-year return period. This means that basing our infrastructure designs on the business-as-usual Atlas 14 could lead to a significant underestimation of precipitation intensities, putting existing and planned infrastructure at elevated risk with uncertain and severe consequences for public safety, infrastructure resilience, and economic stability.

This study also developed IDF curves using 40 future climate realizations (20 GCMs $\times$ 2 RCPs) under stationary and non-stationary conditions following the trend test for one of the DFW stations. The results revealed that irrespective of RCP scenarios, 38 out of 40 GCM-based IDF curves that assumed stationarity showed decreased 24-hour precipitation intensities in any return period. On the other hand, future IDF curves developed based on the non-stationary assumption, irrespective of RCP scenarios, showed an increase in 24-hour precipitation intensities in all return periods by up to 39%. Major finding of this research includes:

- 25% of the stations in DFW metroplex showed non-stationary trend over time.
- Compared to Atlas 14 (stationary), non-stationary IDF curves showed an increase in 24-hour precipitation intensities in all return periods in all 7 stations.
- Majority of future GCMs IDF curve showed a decrease in precipitation intensities in all return periods.

The research findings suggest important implications for water management and infrastructure planning in the DFW metroplex and other similar regions. However, it is worth

noting that this study includes two limitations: virtual cursors for future research direction. Firstly, this study uses time as the only covariate for non-stationarity. As suggested by many scholars, several other factors, such as land use change, topography, atmospheric circulation patterns, greenhouse gas concentrations, etc., can be used as covariates to test their influences on the DFW metroplex climatic conditions. Secondly, using high-resolution and dynamically bias-corrected recent regional climate model ensembles from CMIP-6, specifically for the DFW metroplex, could produce precipitation projections more representative of the Atlas 14 stations in DFW. Addressing these two limitations in future studies may create IDF curves that are adequate to capture varying dynamics of local and regional hydro-meteorological factors and uncertainties related to future climate projections.

In summary, this study may provide important insights into the possible benefits of considering non-stationarity and future climate projections while developing the IDF curve, the critical tool used to design critical hydrological and transportation infrastructures. Creating and using such a climate change adaptive IDF tool for the DFW metroplex and similar urban regions could enable decision-makers to make more informed choices about infrastructure investments, emergency preparedness measures, and long-term planning for urban development and water resource management.

References

Abatzoglou, J. T., & Brown, T. J. (2012). A comparison of statistical downscaling methods suited for wildfire applications. *International Journal of Climatology*, *32*(5), 772-780. https://doi.org/10.1002/joc.2312.

Afriyie, J. K., Twumasi-Ankrah, S., Gyamfi, K. B., Arthur, D., & Pels, W. A. (2020). Evaluating the performance of unit root tests in single time series processes. *Mathematics and Statistics*, *8*(6), 656-664, doi: 10.13189/ms.2020.080605.

AghaKouchak, A., Ragno, E., Love, C., & Moftakhari, H. (2018). Projected Changes in Californias Precipitation Intensity-Duration-Frequency Curves. *California's Fourth Climate Change Assessment*, 32. Available at https://www.energy.ca.gov/sites/default/files/2019-11/CCCA4-CEC-2018 005_ADA.pdf.

Agilan, V., & Umamahesh, N. (2017a). Modelling nonlinear trend for developing non-stationary rainfall intensity–duration–frequency curve. International Journal of Climatology, 37(3), 1265-1281. https://doi.org/10.1002/joc.4774.

Agilan, V., & Umamahesh, N. (2017b). Non-stationary rainfall intensity-duration-frequency relationship: a comparison between annual maximum and partial duration series. *Water Resources Management*, *31*, 1825-1841. https://doi.org/10.1007/s11269-017-1614-9.

Agilan, V., & Umamahesh, N. (2017c). What are the best covariates for developing non-stationary rainfall intensity-duration-frequency relationship? *Advances in Water Resources*, *101*, 11-22. https://doi.org/10.1016/j.advwatres.2016.12.016.

Agilan, V., & Umamahesh, N. (2018). Covariate and parameter uncertainty in non-stationary rainfall IDF curve. *International Journal of Climatology*, *38*(1), 365-383. https://doi.org/10.1002/joc.5181.

Alexander, L. V., Zhang, X., Peterson, T. C., Caesar, J., Gleason, B., Klein Tank, A. M. G., Haylock, M., Collins, D., Trewin, B., Rahimzadeh, F., Tagipour, A., Rupa Kumar, K., Revadekar, J., Griffiths, G., Vincent, L., Stephenson, D. B., Burn, J., Aguilar, E., Brunet, M., . . . Vazquez-Aguirre, J. L. (2006). Global observed changes in daily climate extremes of temperature and precipitation. *Journal of Geophysical Research*, *111*(D5). https://doi.org/10.1029/2005jd006290.

Allan, R. P., Barlow, M., Byrne, M. P., Cherchi, A., Douville, H., Fowler, H. J., Gan, T. Y., Pendergrass, A. G., Rosenfeld, D., & Swann, A. L. (2020). Advances in understanding large-scale responses of the water cycle to climate change. *Annals of the New York Academy of Sciences*, *1472*(1), 49-75. https://doi.org/10.1111/nyas.14337.

Amadeo, K. (2018). Hurricane Harvey facts, damage and costs. *The Balance*. Retrieved from https://www.thebalance.com/hurricane-harvey-facts-damage-costs-4150087.

Arias, P., Bellouin, N., Coppola, E., Jones, R., Krinner, G., Marotzke, J., Naik, V., Palmer, M., Plattner, G.-K., & Rogelj, J. (2021). *Climate Change 2021: The Physical Science Basis. Contribution of Working Group14 I to the Sixth Asses sment Report of the Intergovernmental Panel on Climate Change*. Cambridge University Press. https://www.ipcc.ch/report/ar6/wg1/downloads/report/IPCC_AR6_WGI_SPM_final.pdf.

Armal, S., Porter, J. R., Lingle, B., Chu, Z., Marston, M. L., & Wing, O. E. (2020). Assessing property level economic impacts of climate in the US, new insights and evidence from a comprehensive flood risk assessment tool. *Climate*, *8*(10), 116. https://doi.org/10.3390/cli8100116.

Barber, D. (2012). *Bayesian reasoning and machine learning*. Cambridge University Press.

Berg, P., Moseley, C., & Haerter, J. O. (2013). Strong increase in convective precipitation in response to higher temperatures. *Nature Geoscience*, *6*(3), 181-185. https://doi.org/10.1038/ngeo1731.

Bernard, M. M. (1932). Formulas for rainfall intensities of long duration. *Transactions of the American Society of Civil Engineers*, *96*(1), 592-606. https://doi.org/10.1061/TACEAT.0004323.

Bernardo, J., & Smith, A. (2001). Bayes Theory. Measurement Science & Technology, 12(2), 221-222. https://doi.org/10.1088/0957-0233/12/2/702.

Bonnin, G. M., Martin, D., Lin, B., Parzybok, T., Yekta, M., & Riley, D. (2006). *Precipitation-Frequency Atlas of the United States.* National Oceanic and Atmospheric Administration, National Weather Service, Silver Spring, MD, USA.

Cannon, A. J., & Innocenti, S. (2019). Projected intensification of sub-daily and daily rainfall extremes in convection-permitting climate model simulations over North America: implications for future intensity–duration–frequency curves. *Natural Hazards and Earth System Sciences*, *19*(2), 421-440. https://doi.org/10.5194/nhess-19-421-2019.

Chandra, R., Saha, U., & Mujumdar, P. (2015). Model and parameter uncertainty in IDF relationships under climate change. *Advances in Water Resources*, *79*, 127-139. https://doi.org/10.1016/j.advwatres.2015.02.011.

Chen, X., Zhang, H., Chen, W., & Huang, G. (2021). Urbanization and climate change impacts on future flood risk in the Pearl River Delta under shared socioeconomic pathways. *Science of the Total Environment*, *762*, 143144. https://doi.org/10.1016/j.scitotenv.2020.143144.

Cheng, L., & Aghakouchak, A. (2015). Non-stationary Precipitation Intensity-Duration-Frequency Curves for Infrastructure Design in a Changing Climate. *Scientific Reports*, *4*(1), 7093. https://doi.org/10.1038/srep07093.

Cheng, L., Aghakouchak, A., Gilleland, E., & Katz, R. W. (2014). Non-stationary extreme value analysis in a changing climate. *Climatic Change*, *127*(2), 353-369. https://doi.org/10.1007/s10584-014-1254-5.

Cheung, Y.-W., & Lai, K. S. (1995). Lag order and critical values of the augmented Dickey–Fuller test. *Journal of Business & Economic Statistics*, *13*(3), 277-280. https://doi.org/10.1080/07350015.1995.10524601.

Chow, K. V., & Denning, K. C. (1993). A simple multiple variance ratio test. *Journal of econometrics*, 58(3), 385-401. https://doi.org/10.1016/0304-4076(93)90051-6.

Chris, R. (2015). DFW: Heavy rain, thunderstorms, & flash flooding Memorial Weekend. iweathernet.com. Retrieved from https://www.iweathernet.com/dallas-fort-worth/dfw-heavy-rain-thunderstorms-flash-flooding-memorial-weekend.

Coles, S., Springer, & SpringerLink. (2001). *An Introduction to Statistical Modeling of Extreme Values*. *Springer London*. [eBook]. https://go.exlibris.link/HLtQdgHf.

Conte, L. C., Bayer, D. M., & Bayer, F. M. (2019). Bootstrap Pettitt test for detecting change points in hydroclimatological data: case study of Itaipu Hydroelectric Plant, Brazil. *Hydrological Sciences Journal*, *64*(11), 1312-1326. https://doi.org/10.1080/02626667.2019.1632461.

Cooley, D., Nychka, D., & Naveau, P. (2007). Bayesian Spatial Modeling of Extreme Precipitation Return Levels. *Journal of the American Statistical Association*, *102*(479), 824-840. https://doi.org/10.1198/016214506000000780.

Cotter, J. L. (2018). Extreme Precipitation, NOAA Atlas 14, Other InFRM Initiatives What Can You Do? [Conference session]. TX Civil Engineering Conference, San Marcos, TX. Retrieved from https://www.ci.buda.tx.us/DocumentCenter/View/6577/CECON-2018-NOAA-Atlas-14-Presentation-J-Cotter-USACE.

Cox, S. (2006). A developed ideal emergency management program setting and plan: *A case study of Navarro County*. Unpublished master's thesis, Texas A&M University-Commerce.

Damberg, L., & Aghakouchak, A. (2014). Global trends and patterns of drought from space. *Theoretical and Applied Climatology*, 117(3-4), 441-448. DOI: https://doi.org/10.1007/s00704-013-1019-5.

Davis, R. (2021, May 19). *USA-Emergency declared after floods in Louisiana*. FloodList. https://floodlist.com/america/usa/floods-louisiana-texas-may-2021.

DeGaetano, A. T., & Castellano, C. M. (2017). Future projections of extreme precipitation intensity-duration-frequency curves for climate adaptation planning in New York State. *Climate Services*, *5*(1), 23-35. https://doi.org/10.1016/j.cliser.2017.03.003.

Dewan, A. (2021, August 4). *Germany's deadly floods were up to 9 times more likely because of climate change, study estimates*. CNN World. https://www.cnn.com/2021/08/23/europe/germany-floods-belgium-climate-change-intl/index.html.

Dey, S., & Douglas, E. (2022, August 22). *Flooding hits Dallas-Fort Worth as some areas receive more than 13 inches of rain*. Weatherford Democrat. https://www.texastribune.org/2022/08/22/dallas-flooding-fort-worth.

Easterling, D.R., K.E. Kunkel, J.R. Arnold, T. Knutson, A.N. LeGrande, L.R. Leung, R.S. Vose, D.E. Waliser, and M.F. Wehner, (2017). Precipitation change in the United States. In: *Climate Science Special Report: Fourth National Climate Assessment, Volume I* [Wuebbles, D.J., D.W. Fahey, K.A. Hibbard, D.J. Dokken, B.C. Stewart, and T.K. Maycock (eds.)]. U.S. Global Change Research Program, Washington, DC, USA, pp. 207-230, doi: 10.7930/J0H993CC.

Elliott, G., Rothenberg, T. J., & Stock, J. H. (1992). Efficient tests for an autoregressive unit root. In: *National Bureau of Economic Research*. Cambridge, Mass., USA.

Emanuel, K. (2017). Assessing the present and future probability of Hurricane Harvey's rainfall. *Proceedings of the National Academy of Sciences*, *114*(48), 12681-12684. https://doi.org/10.1073/pnas.1716222114.

Feng, B., Zhang, Y., & Bourke, R. (2021). Urbanization impacts on flood risks based on urban growth data and coupled flood models. *Natural Hazards*, *106*(1), 613-627. https://doi.org/10.1007/s11069-020-04480-0.

Fischer, E. M., & Knutti, R. (2016). Observed heavy precipitation increase confirms theory and early models. *Nature Climate Change*, *6*(11), 986-991. https://doi.org/10.1038/nclimate3110.

Ganguli, P., & Coulibaly, P. (2017). Does nonstationarity in rainfall require non-stationary intensity–duration–frequency curves? *Hydrology and Earth System Sciences*, *21*(12), 6461-6483. https://doi.org/10.5194/hess-21-6461-2017.

Groisman, P. Y., Knight, R. W., Easterling, D. R., Karl, T. R., Hegerl, G. C., & Razuvaev, V. N. (2005). Trends in Intense Precipitation in the Climate Record. *Journal of Climate*, *18*(9), 1326-1350. https://doi.org/10.1175/jcli3339.1.

Hashmi, M. Z., Shamseldin, A. Y., & Melville, B. W. (2013). Statistically downscaled probabilistic multi-model ensemble projections of precipitation change in a watershed. *Hydrological processes*, *27*(7), 1021-1032, doi: 10.1002/hyp.8413.

Hershfield, D. M. (1961). Rainfall frequency atlas of the United States. *Technical paper*, *40*, 1-61. https://biotech.law.lsu.edu/blog/TechnicalPaper_No40.pdf.

Hossain, I., Khastagir, A., Aktar, M., Imteaz, M., Huda, D., & Rasel, H. (2021). Comparison of estimation techniques for generalised extreme value (GEV) distribution parameters:

a case study with Tasmanian rainfall. *International Journal of Environmental Science and Technology*, 1-14, doi:10.1007/s13762-021-03693-5.

Houck, K., & Board, C. W. C. (2019). Projecting Rainfall Intensity Duration Frequency Curves Under Climate Change. Retrieved from https://waterinfo.org/wp-content/uploads/2020/02/CWCB-IDF-Curve-Projection-Paper-Final.pdf.

Hsiang, S., Kopp, R., Jina, A., Rising, J., Delgado, M., Mohan, S., Rasmussen, D., Muir-Wood, R., Wilson, P., & Oppenheimer, M. (2017). Estimating economic damage from climate change in the United States. *Science*, *356*(6345), 1362-1369. https://www.science.org/doi/10.1126/science.aal4369.

Ian, T. (2023). Cumulative CO_2 emissions from fossil fuel combustion worldwide 1750-2021, by country. Statista. Retrieved from https://www.statista.com/statistics/1007454/cumulative-co2-emissions-worldwide-by-country/.

Intergovernmental Panel on Climate Change (IPCC). (2002). *IPCC workshop report on changes in extreme weather and climate events*, Beijing, China, 11–13 June, 2002. https://archive.ipcc.ch/pdf/supporting-material/ipcc-workshop-2002-06.pdf.

IPCC. (2021). Summary for Policymakers. In: *Climate Change 2021: The Physical Science Basis. Contribution of Working Group I to the Sixth Assessment Report of the Intergovernmental Panel on Climate Change*. Masson-Delmotte, V., Zhai, P., Pirani, A., Connors, S.L., Péan, C., Berger, S., Caud, N., Chen, Y., Goldfarb, L., Gomis, M.I., Huang, M., Leitzell, K., Lonnoy, E., Matthews, J.B.R., Maycock, T.K., Waterfield, T., Yelekçi, O., Yu, R., and Zhou, B. (Eds.). *Cambridge University Press*. doi:10.1017/9781009157896.001. (pp. 3-32).

Kendall, M. G. (1948). *Rank correlation methods*. London, England: Charles Griffin.

Klein Tank, A. M. G., & Können, G. P. (2003). Trends in Indices of Daily Temperature and Precipitation Extremes in Europe, 1946–99. *Journal of Climate*, *16*(22), 3665-3680. https://doi.org/10.1175/1520-0442(2003)016<3665:tiiodt>2.0.co;2.

Kreienkamp, F., Philip, S. Y., Tradowsky, J. S., Kew, S. F., Lorenz, P., Arrighi, J., Belleflamme, A., Bettmann, T., Caluwaerts, S., & Chan, S. C. (2021). Rapid attribution of heavy rainfall events leading to the severe flooding in Western Europe during July 2021. *World Weather Attribution.* [online]. Available at: https://www.worldweatherattribution.org/heavy-rainfall-western-europe-july-2021/.

Kunkel, K. E. (2003). The Link between Extreme Precipitation and Flooding. Natural Hazards, 29(2), 291-305. https://doi.org/10.1023/a:1023694115864.

Kwiatkowski, D., Phillips, P. C., Schmidt, P., & Shin, Y. (1992). Testing the null hypothesis of stationarity against the alternative of a unit root: How sure are we that economic time series have a unit root? *Journal of econometrics*, *54*(1-3), 159-178. http://dx.doi.org/10.1016/0304-4076(92)90104-Y.

Lanning-Rush, J., Asquith, W. H., & Slade, R. M. (1998). *Extreme precipitation depths for Texas, excluding the Trans-Pecos region* (Vol. 98). US Department of the Interior, US Geological Survey.

Lee, K., & Singh, V. P. (2020). Analysis of uncertainty and non-stationarity in probable maximum precipitation in Brazos River basin. *Journal of Hydrology*, *590*, 125526. https://doi.org/10.1016/j.jhydrol.2020.125526.

Lezama Valdes, L.-M., Katurji, M., & Meyer, H. (2021). A Machine Learning Based Downscaling Approach to Produce High Spatio-Temporal Resolution Land Surface Temperature of the Antarctic Dry Valleys from MODIS Data. *Remote Sensing*, *13*(22), 4673. https://doi.org/10.3390/rs13224673.

Li, X., & Hu, Q. (2019). Spatiotemporal changes in extreme precipitation and its dependence on topography over the Poyang Lake Basin, China. *Advances in Meteorology*, *2019*. https://doi.org/10.1155/2019/1253932.

Liu, J., & Niyogi, D. (2019). Meta-analysis of urbanization impact on rainfall modification. *Scientific Reports*, *9*(1), 1-14. https://doi.org/10.1038/s41598-019-42494-2.

Liu, S., Xie, Y., Fang, H., Du, H., & Xu, P. (2022). Trend Test for Hydrological and Climatic Time Series Considering the Interaction of Trend and Autocorrelations. *Water*, *14*(19), 3006. https://doi.org/10.3390/w14193006.

Ljung, G. M., & Box, G. E. (1978). On a measure of lack of fit in time series models. *Biometrika, 65*(2), 297-303. https://doi.org/10.1093/biomet/65.2.297.

Lopez-Cantu, T., Prein, A. F., & Samaras, C. (2020). Uncertainties in future US extreme precipitation from downscaled climate projections. *Geophysical Research Letters*, *47*(9). https://doi.org/10.1029/2019GL086797.

Luu, L. N., Scussolini, P., Kew, S., Philip, S., Hariadi, M. H., Vautard, R., Van Mai, K., Van Vu, T., Truong, K. B., & Otto, F. (2021). Attribution of typhoon-induced torrential precipitation in Central Vietnam, October 2020. *Climatic Change*, *169*(3-4), 1-22. https://doi.org/10.1007/s10584-021-03261-3.

Macro Trends, U. (2023). *Dallas-Fort Worth Metro Area Population 1950-2023*. [online]. Available at: https://www.macrotrends.net/cities/22966/dallas-fort-worth/population.

Mann, H. B. (1945). Nonparametric tests against trend. *Econometrica: Journal of the econometric society*, 245-259. http://dx.doi.org/10.2307/1907187.

Markolf, S. A., Chester, M. V., Helmrich, A. M., & Shannon, K. (2021). Re-imagining design storm criteria for the challenges of the 21st century. *Cities*, *109*, 102981. https://doi.org/10.1016/j.cities.2020.102981.

Marra, F., Armon, M., & Morin, E. (2022). Coastal and orographic effects on extreme precipitation revealed by weather radar observations. *Hydrology and Earth System Sciences*, *26*(5), 1439-1458. https://doi.org/10.5194/hess-26-1439-2022.

Masson-Delmotte, V., Zhai, P., Pirani, A., Connors, S. L., Péan, C., Berger, S., Caud, N., Chen, Y., Goldfarb, L., & Gomis, M. (2021). *Climate Change 2021: The Physical Science Basis.* Contribution of Working Group I to the Sixth Assessment Report of the Intergovernmental Panel on Climate Change, Chapter 2. IPCC. [online] Available at: https://www.ipcc.ch/report/ar6/wg1/downloads/report/IPCC_AR6_WGI_Chapter_02.pdf.

Miller, J. F., Frederick, R. H., & Tracey, R. J. (1973). *Precipitation-Frequency Atlas of the Western United States, Volume 3: Colorado*. [online] US Department of Commerce, National Oceanic and Atmospheric Administration, Environmental Data Service. Available at: https://repository.library.noaa.gov/view/noaa/22624/noaa 22624_DS1.pdf.

Miro, M. E., DeGaetano, A. T., López-Cantú, T., Samaras, C., Webber, M., & Romita Grocholski, K. (2021). *Developing Future Projected Intensity-Duration-Frequency (IDF) Curves: A Technical Report on Data, Methods, and IDF Curves for the Chesapeake Bay Watershed and Virginia.* RAND Corporation. https://doi.org/10.7249/TLA1365-1.

Moss, R. H., Kravitz, B., Delgado, A., Asrar, G., Brandenbeger, J., Wigmosta, M., Preston, K., Buzan, T., Gremillion, M., & Shaw, P. (2017). *Nonstationarity RC Workshop Report: Non-stationary Weather Patterns and Extreme Events Informing Design and Planning for Long-Lived Infrastructure* [Report]. Academia.edu. https://www.academia.edu/91224896/Nonstationarity_RC_Workshop_Report_Nonstationary_Weather_Patterns_and_Extreme_Events_Informing_Design_and_Planning_for_Long_Lived_Infrastructure.

NCTCOG. (2015). *Navarro County Hazard Mitigation Action Plan*. Retrieved from https://www.nctcog.org/getmedia/c15b6455-8bd5-4eaf-b83e-e534e93b7aad/navarro-county-approved-hazmap.pdf

Nielsen-Gammon, J., Escobedo, J., Ott, C., Dedrick, J., & Van Fleet, A. (2020). *Assessment of historic and future trends of extreme weather in Texas, 1900-2036*. Retrieved from https://climatexas.tamu.edu/files/ClimateReport-1900to2036-2021Update.

NOAA. (2018, September 27). *NOAA updates Texas rainfall frequency values.* NOAA. https://www.noaa.gov/media-release/noaa-updates-texas-rainfall-frequency-values.

NOAA National Centers for Environmental Information (NCEI). (2022). *U.S. Billion-Dollar Weather and Climate Disasters (2022)*. https://www.ncei.noaa.gov/access/billions/, doi: 10.25921/stkw-7w73.

National Oceanic and Atmospheric Administration (NOAA). (2021). *Climate at a glance*. In: NOAA Silver Spring, MD.

Noto, L., Cipolla, G., Pumo, D., & Francipane, A. (2023). Climate Change in the Mediterranean Basin (Part II): A Review of Challenges and Uncertainties in Climate Change Modeling and Impact Analyses. *Water Resources Management*, 1-17. https://doi.org/10.1007/s11269-023-03444-w.

O'Neill, B. C., Tebaldi, C., Van Vuuren, D. P., Eyring, V., Friedlingstein, P., Hurtt, G., Knutti, R., Kriegler, E., Lamarque, J.-F., & Lowe, J. (2016). The scenario model intercomparison project (ScenarioMIP) for CMIP6. *Geoscientific Model Development*, *9*(9), 3461-3482. https://doi.org/10.5194/gmd-9-3461-2016.

Ouarda, T. B. M. J., Yousef, L. A., & Charron, C. (2019). Non-stationary intensity-duration-frequency curves integrating information concerning teleconnections and climate change. *International Journal of Climatology*, *39*(4), 2306-2323. https://doi.org/10.1002/joc.5953.

Park, J. S., Kang, H. S., Lee, Y. S., & Kim, M. K. (2011). Changes in the extreme daily rainfall in South Korea. *International Journal of Climatology*, *31*(15), 2290-2299, doi:10.1002/joc.2236.

Patra, S., Sahoo, S., Mishra, P., & Mahapatra, S. C. (2018). Impacts of urbanization on land use/cover changes and its probable implications on local climate and groundwater level. *Journal of urban management*, *7*(2), 70-84, doi:10.1016/j.jum.2018.04.006.

Paul, S., Ghebreyesus, D., & Sharif, H. O. (2019). Brief communication: Analysis of the fatalities and socio-economic impacts caused by Hurricane Florence. *Geosciences*, *9*(2), 58. https://doi.org/10.3390/geosciences9020058.

Pendergrass, A. G., Lehner, F., Sanderson, B. M., & Xu, Y. (2015). Does extreme precipitation intensity depend on the emissions scenario? *Geophysical Research Letters*, *42*(20), 8767-8774. https://doi.org/10.1002/2015gl065854.

Perica, S., Pavlovic, S., St Laurent, M., Trypaluk, C., Unruh, D., & Wilhite, O. (2018). *Precipitation-Frequency Atlas of the United States*. Volume 11, Version 2.0. Texas. https://doi.org/10.25923/1ceg-5094.

Pettitt, A. N. (1979). A non-parametric approach to the change-point problem. *Journal of the Royal Statistical Society: Series C (Applied Statistics)*, *28*(2), 126-135. https://doi.org/10.2307/2346729.

Phillips, P. C., & Perron, P. (1988). Testing for a unit root in time series regression. *Biometrika*, *75*(2), 335-346. https://doi.org/10.2307/2336182.

Prosdocimi, I., Kjeldsen, T., & Svensson, C. (2014). Non-stationarity in annual and seasonal series of peak flow and precipitation in the UK. *Natural Hazards and Earth System Sciences*, *14*(5), 1125-1144. https://doi.org/10.5194/nhess-14-1125-2014.

Ragno, E., AghaKouchak, A., Cheng, L., & Sadegh, M. (2019). A generalized framework for process-informed non-stationary extreme value analysis. *Advances in Water Resources*, *130*, 270-282. https://doi.org/10.1016/j.advwatres.2019.06.007.

Ragno, E., Aghakouchak, A., Love, C. A., Cheng, L., Vahedifard, F., & Lima, C. H. R. (2018). Quantifying Changes in Future Intensity-Duration-Frequency Curves Using Multimodel Ensemble Simulations. *Water Resources Research*, *54*(3), 1751-1764. https://doi.org/10.1002/2017wr021975.

Rajendran, V., Dhanya, C. T., & Chaudhary, S. (2019). Covariate based Time-Varying Intensity-Duration-Frequency Curve for Changing Climate. *Geophysical Research Abstracts (Vol. 21),* EGU2019-14723-1, 2019. https://ui.adsabs.harvard.edu/abs/2019EGUGA..2114723R/abstract.

Ren, H., Hou, Z. J., Wigmosta, M., Liu, Y., & Leung, L. R. (2019). Impacts of spatial heterogeneity and temporal non-stationarity on intensity-duration-frequency estimates—a case study in a mountainous california-nevada watershed. *Water*, *11*(6), 1296. https://doi.org/10.3390/w11061296.

Riahi, K., Rao, S., Krey, V., Cho, C., Chirkov, V., Fischer, G., Kindermann, G., Nakicenovic, N., & Rafaj, P. (2011). RCP 8.5—A scenario of comparatively high greenhouse gas emissions. *Climatic Change*, *109*(1), 33-57. https://doi.org/10.1007/s10584-011-0149-y.

Ritchie, H., Roser, M., & Rosado, P. (2020). CO_2 and greenhouse gas emissions. *Our world in data*. Available at https://ourworldindata.org/co2-and-other-greenhouse-gas-emissions. [Accessed 25 April 2023].

Robert, C. P. (2007). *The Bayesian choice: from decision-theoretic foundations to computational implementation (Vol. 2).* Springer. https://errorstatistics.files.wordpress.com/2016/03/robert-20071.pdf.

Roderick, T. P., Wasko, C., & Sharma, A. (2020). An improved covariate for projecting future rainfall extremes? *Water Resources Research*, *56*(8), e2019WR026924. https://doi.org/10.1029/2019WR026924.

Rougé, C., Ge, Y., & Cai, X. (2013). Detecting gradual and abrupt changes in hydrological records. *Advances in Water Resources*, *53*, 33-44. https://doi.org/10.1016/j.advwatres.2012.09.008.

Runkle, J., Kunkel, K., Nielsen-Gammon, J., Frankson, R., Champion, S., Stewart, B., Romolo, L., & Sweet, W. (2022). Texas state climate summary 2022. *NOAA Technical Report NESDIS 150-TX*, *NOAA/NESDIS,* Silver Spring, *MD*, 1-5.

Rypkema, D., & Tuljapurkar, S. (2021). Modeling extreme climatic events using the generalized extreme value (GEV) distribution. In *Handbook of Statistics (Vol. 44*, pp. 39-71). Elsevier, doi:10.1016/bs.host.2020.12.002.

Sam, M. G., Nwaogazie, I. L., & Ikebude, C. (2022). Non-Stationary Trend Change Point Pattern Using 24-Hourly Annual Maximum Series (AMS) Precipitation Data. *Journal of Water Resource and Protection*, *14*(8), 592-609, doi: 10.4236/jwarp.2022.148031.

Sarkar, S., & Maity, R. (2021). Global climate shift in 1970s causes a significant worldwide increase in precipitation extremes. *Scientific Reports*, *11*(1). https://doi.org/10.1038/s41598-021-90854-8.

Shrestha, A., Babel, M., Weesakul, S., & Vojinovic, Z. (2017). Developing Intensity–Duration–Frequency (IDF) Curves under Climate Change Uncertainty: The Case of Bangkok, Thailand. *Water*, *9*(2), 145. https://doi.org/10.3390/w9020145.

Shukor, M. S. A., Yusop, Z., Yusof, F., Sa'Adi, Z., & Alias, N. E. (2020). Detecting Rainfall Trend and Development of Future Intensity Duration Frequency (IDF) Curve for the State of Kelantan. *Water Resources Management*, *34*(10), 3165-3182. https://doi.org/10.1007/s11269-020-02602-8.

Silva, D. F., Simonovic, S. P., Schardong, A., & Goldenfum, J. A. (2021). Assessment of non-stationary IDF curves under a changing climate: Case study of different climatic zones in Canada. *Journal of Hydrology: Regional Studies*, *36*, 100870. https://doi.org/10.1016/j.ejrh.2021.100870.

Singh, J., Karmakar, S., PaiMazumder, D., Ghosh, S., & Niyogi, D. (2020). Urbanization alters rainfall extremes over the contiguous United States. *Environmental Research Letters*, *15*(7), 074033, doi: 10.1088/1748-9326/ab8980.

Smith, A., Lott, N., Houston, T., Shein, K., Crouch, J., & Enloe, J. (2021). US Billion-Dollar Weather & Climate Disasters 1980-2021. *NOAA National Centers for Environmental Information: Asheville, NC, USA*, *15*.

Solomon, S., Qin, D., Manning, M., Averyt, K., & Marquis, M. (2007). *Climate change 2007-the physical science basis: Working group I contribution to the fourth assessment report of the IPCC* (Vol. 4). Cambridge university press.

Song, X., Mo, Y., Xuan, Y., Wang, Q. J., Wu, W., Zhang, J., & Zou, X. (2021). Impacts of urbanization on precipitation patterns in the greater Beijing–Tianjin–Hebei metropolitan region in northern China. *Environmental Research Letters*, *16*(1), 014042, doi:10.1088/1748-9326/abd212.

Soulis, E. D., Sarhadi, A., Tinel, M., & Suthar, M. (2016). Extreme precipitation time trends in Ontario, 1960-2010. *Hydrological processes*, *30*(22), 4090-4100. https://doi.org/10.1002/hyp.10969.

Soumya, R., Anjitha, U., Mohan, S., Adarsh, S., & Gopakumar, R. (2020). Incorporation of non-stationarity in precipitation intensity-duration-frequency curves for Kerala, India. *IOP Conference Series: Earth and Environmental Science 491* (1), 012013, doi:10.1088/1755-1315/491/1/012013.

Sterzel, T., Lüdeke, M. K., Walther, C., Kok, M. T., Sietz, D., & Lucas, P. L. (2020). Typology of coastal urban vulnerability under rapid urbanization. *PLoS One*, *15*(1), e0220936. https://doi.org/10.1371/journal.pone.0220936.

Sun, Q., Miao, C., Qiao, Y., & Duan, Q. (2017). The non-stationary impact of local temperature changes and ENSO on extreme precipitation at the global scale. *Climate Dynamics*, *49*(11), 4281-4292. https://doi.org/10.1007/s00382-017-3586-0.

Swinburne, R. (2004). Bayes' theorem. *Revue Philosophique de la France Et de l*, *194*(2), doi:10.1093/mind/113.451.591.

Tabari, H. (2020). Climate change impact on flood and extreme precipitation increases with water availability. *Scientific Reports*, *10*(1). https://doi.org/10.1038/s41598-020-70816-2.

Team, F. M. A. (2006). *Hurricane Katrina in the Gulf Coast-Mitigation Assessment Team Report: Building Performance Observations, Recommendations, and Technical Guidance*. Washington, DC: Federal Emergency Management Agency (FEMA).

Texas Water Development Board, T. (2022). *2022 State Water Plan. Water for Texas*. Retrieved from www.twdb.texas.gov/waterplanning/swp/2022

Thomson, A. M., Calvin, K. V., Smith, S. J., Kyle, G. P., Volke, A., Patel, P., Delgado-Arias, S., Bond-Lamberty, B., Wise, M. A., & Clarke, L. E. (2011). RCP4. 5: a pathway for stabilization of radiative forcing by 2100. *Climatic Change*, *109*(1), 77-94. https://doi.org/10.1007/s10584-011-0151-4.

Thrasher, B., Wang, W., Michaelis, A., Melton, F., Lee, T., & Nemani, R. (2022). NASA global daily downscaled projections, CMIP6. *Scientific Data*, *9*(1), 262. https://doi.org/10.1038/s41597-022-01393-4.

Tien Thanh, N., & Dutto Aldo Remo, L. (2018). Projected Changes of Precipitation IDF Curves for Short Duration under Climate Change in Central Vietnam. *Hydrology*, *5*(3), 33. https://doi.org/10.3390/hydrology5030033.

Towler, E., Rajagopalan, B., Gilleland, E., Summers, R. S., Yates, D., & Katz, R. W. (2010). Modeling hydrologic and water quality extremes in a changing climate: A statistical approach based on extreme value theory. *Water Resources Research*, *46*(11), n/a-n/a. https://doi.org/10.1029/2009wr008876.

Trenberth, K. (2011). Changes in precipitation with climate change. *Climate Research*, *47*(1), 123-138. https://doi.org/10.3354/cr00953.

Um, M.-J., Heo, J.-H., Markus, M., & Wuebbles, D. J. (2018). Performance evaluation of four statistical tests for trend and non-stationarity and assessment of observed and projected annual maximum precipitation series in Major United States cities. *Water Resources Management*, *32*, 913-933. https://doi.org/10.1007/s11269-017-1846-8.

Underwood, B. S., Guido, Z., Gudipudi, P., & Feinberg, Y. (2017). Increased costs to US pavement infrastructure from future temperature rise. *Nature Climate Change*, *7*(10), 704-707. https://doi.org/10.1038/nclimate3390.

United Nations Department of Economic and Social Affairs, Population. Divsion. (2021). *Global Population Growth and Sustainable Development*. Retrieved from https://population.un.org/wpp/Publications/Files/WPP2020_Booklet.pdf

Vahedifard, F., Tehrani, F. S., Galavi, V., Ragno, E., & AghaKouchak, A. (2017). Resilience of MSE walls with marginal backfill under a changing climate: Quantitative assessment for extreme precipitation events. *Journal of Geotechnical and Geoenvironmental Engineering*, *143*(9), 04017056. https://doi.org/10.1061/(ASCE)GT.1943-5606.0001743.

Villarini, G., Taylor, S., Wobus, C., Vogel, R., Hecht, J., White, K., Baker, B., Gilroy, K., Olsen, R., & Raff, D. (2018). Floods and nonstationarity-A review. *USACE Climate preparedness and resilience, CWTS*, *1*(2018), 30. Available at https://sites.tufts.edu/richardvogel/files/2019/04/2018_floodsAndNonstationarity.pdf.

Von Sachs, R., & Neumann, M. H. (2000). A wavelet-based test for stationarity. *Journal of time series analysis, 21*(5), 597-613. https://doi.org/10.1111/1467-9892.00200.

Walsh, J., Anderson, D., Doney, S., Feely, R., Hennon, P., Kharin, V., Knutson, T., Landerer, F., Lenton, T., Kennedy, J., & Somerville, R. (2014). *Climate Change Impacts in the United States*. https://doi.org/10.7930/J0KW5CX.

Weber, H., & Sciubba, J. D. (2019). The Effect of Population Growth on the Environment: Evidence from European Regions. *European Journal of Population*, *35*(2), 379-402. https://doi.org/10.1007/s10680-018-9486-0.

Whan, K., & Zwiers, F. (2017). The impact of ENSO and the NAO on extreme winter precipitation in North America in observations and regional climate models. *Climate Dynamics*, *48*(5), 1401-1411. https://doi.org/10.1007/s00382-016-3148-x.

Wi, S., Valdés, J. B., Steinschneider, S., & Kim, T.-W. (2016). Non-stationary frequency analysis of extreme precipitation in South Korea using peaks-over-threshold and annual maxima. *Stochastic Environmental Research and Risk Assessment*, *30*(2), 583-606. https://doi.org/10.1007/s00477-015-1180-8.

Winguth, A., Lee, J. H., & Ko, Y. (2015). *Climate change/extreme weather vulnerability and risk assessment for transportation infrastructure in Dallas and Tarrant counties*. In North Central Texas Council of Governments. Avaibale at https://climateresearchgroup.uta.edu/Research/NCTCOG_FHWAClimateChangePilot_RevisedFinal_3-24-15.pdf.

Wood, A. W., Maurer, E. P., Kumar, A., & Lettenmaier, D. P. (2002). Long-range experimental hydrologic forecasting for the eastern United States. *Journal of*

Geophysical Research: Atmospheres, *107*(D20), ACL 6-1-ACL 6-15. https://doi.org/10.1029/2001JD000659.

Wootten, A., Terando, A., Reich, B. J., Boyles, R., & Semazzi, F. (2017). Characterizing sources of uncertainty from global climate models and downscaling techniques. *Journal of Applied Meteorology and Climatology*, *56*(12), 3245-3262. https://doi.org/10.1175/JAMC-D-17-0087.1.

Xu, Z., Han, Y., Tam, C.-Y., Yang, Z.-L., & Fu, C. (2021). Bias-corrected CMIP6 global dataset for dynamical downscaling of the historical and future climate (1979–2100). *Scientific Data*, *8*(1), 293. https://doi.org/10.1038/s41597-021-01079-3.

Zalina, M. D., Desa, M. N. M., Nguyen, V., & Kassim, A. H. M. (2002). Selecting a probability distribution for extreme rainfall series in Malaysia. *Water science and technology*, *45*(2), 63-68. https://doi.org/10.2166/wst.2002.0028.

Zhao, Y., Chen, D., Li, J., Chen, D., Chang, Y., Li, J., & Qin, R. (2020). Enhancement of the summer extreme precipitation over North China by interactions between moisture convergence and topographic settings. *Climate Dynamics*, *54*, 2713-2730. https://doi.org/10.1007/s00382-020-05139-z.

Zhou, Q., Leng, G., Su, J., & Ren, Y. (2019). Comparison of urbanization and climate change impacts on urban flood volumes: Importance of urban planning and drainage adaptation. *Science of the Total Environment*, *658*, 24-33. https://doi.org/10.1016/j.scitotenv.2018.12.184.

Zivot, E., & Andrews, D. W. K. (2002). Further evidence on the great crash, the oil-price shock, and the unit-root hypothesis. *Journal of Business & Economic Statistics, 20*(1), 25-44. https://doi.org/10.1198/073500102753410372.

Vita

Binita Ghimire, daughter of Bishow Nath Ghimire (late) and Sushila Ghimire, is a passionate and accomplished individual with a background in agricultural and environmental sciences. Born in Nawalparasi and raised in Lamjung, Nepal, Binita's academic journey has taken her to the National School of Sciences in Kathmandu, where she earned an associate degree, and to the Tribhuvan University Lamjung, where she received a Bachelor of Science in agricultural sciences. She is pursuing a Master of Science in Environmental Science in Texas Christian University, Fort Worth, Texas, where she has also worked as a Teaching Assistant and IT Support Specialist.

Binita has gained valuable experience working as a Homestead Food Production Trainee with Helen Keller International in Nepal, where she developed a deep understanding of sustainable agriculture practices. At TCU, she developed her skills in data analysis and python programming, making her a valuable asset to any organization. Binita's communication skills in two languages (English and Nepali) enable her to convey complex information and collaborate with diverse teams effectively. Her passion for environmental sustainability and her knowledge of environmental regulations and policies further underscores her commitment to positively impacting the world.

Binita's dedication to her academic and professional pursuits is a testament to her work ethic and determination. Her broad range of skills and experiences, and her deep interest in agriculture, make her an ideal candidate for organizations that prioritize eco-consciousness and social responsibility.

She is married to Roshan Adhikari of Lamjung, Nepal.

Abstract

NON-STATIONARY AND CLIMATE CHANGE-INFORMED INTENSITY-

DURATION-FREQUENCY (IDF) CURVE FOR THE DALLAS-FORT WORTH

METROPLEX, TEXAS, UNITED STATES

by

Binita Ghimire

Master of Environmental Science, 2023
Department of Environmental Sciences and Sustainability
Texas Christian University

Thesis Advisor: Gehendra Kharel, Assistant Professor of Environmental and Sustainability

Sciences

Extreme precipitation is becoming more frequent and intense due to climate change. Nonetheless, the infrastructure design tools such as Intensity-Duration-Frequency (IDF) curves still rely on historical precipitation and stationary assumption, risking current and future urban infrastructure. This study developed IDF curves by incorporating non-stationarity trends in precipitation records and Global Climate Models (GCMs)-based precipitation ensembles for the Dallas-Fort Worth metroplex, Texas, United States. A Pro-NEVA tool was utilized to develop seven IDF curves taking historical precipitation annual maximum series for seven out of 88 stations that showed a non-stationary trend with time as a covariate. Also, 40 future climate-based IDF curves (20 GCMs $\times$ 2 RCPs) were developed for one of the DFW stations. IDF curves, constructed with historical precipitation records and under the non-stationary assumption, indicated an increase (up to 75%) in the 24-hour precipitation intensity for the 100-year return period. While only 5% of the IDF curves, constructed using projected GCM

precipitation, showed an increase (up to 39%) in the 24-hour precipitation intensity for any return period. Creating and using such a climate change adaptive IDF tool for the DFW metroplex and similar urban regions could enable decision-makers to make climate-informed choices about infrastructure investments, emergency preparedness measures, and long-term planning for urban development and water resource management.